50P

SYSTEMS DESIGN OF SPACE SIMULATOR CHAMBERS

Prepared For Inclusion

In An AGARDograph Entitled

"SPACE SIMULATION CHAMBERS AND TECHNIQUES"

By

W. R. Howard

June 11, 1963

Submitted for Publication

California Institute of Technology
Jet Propulsion Laboratory
Pasadena, ~~California~~

TABLE OF CONTENTS

FIGURES

I. INTRODUCTION

For a number of years, specialized environmental test facilities have been developed to simulate effects of very high altitude. Examples of these facilities are cold rooms, high altitude vacuum chambers and solar radiation ovens. With the advent of the space exploration program, the performance of conventional high altitude facilities were extended to lower pressures and colder wall temperatures to better simulate space orbital conditions. Facilities then began to appear which simultaneously simulated both the vacuum and heat sink of space. Recently, as spacecraft design has grown more sophisticated, the requirement to add solar simulation has emerged.

At the present time, vacuum and cryogenic technology has progressed fairly well along. Conversely, the current state-of-the-art in producing a large well-collimated sunlight beam with an adequate energy spectrum is in it's infancy.

Another new challenging space simulator design problem is how to simultaneously produce the three major effects of space where heretofore only one or two effects were provided in a single facility. It is evident that many interactions occur between these major subsystems and these interface problems must be solved in the overall system design. In view of the present situation, the author proposes that this chapter be devoted to highlighting some of the typical subsystem interactions and performance tradeoff considerations that should be included in the system design activity. In keeping with this theme, only large facilities simulating at least three characteristics of space will be considered (i.e., vacuum, heat sink, and solar radiation.).

Since the design and performance characteristics of individual subsystems are well described in the preceding chapters, specific design features discussed herein will ~~be limited~~ to those which illustrate system design problems.

II. VACUUM CHAMBER OR PRESSURE VESSEL DESIGN

1. Effects of Vacuum Performance Specification on Design of a Pressure Vessel

One of the most important specifications controlling the design of the vacuum chamber or pressure vessel is the ultimate vacuum level required. Although there is no evidence that ultra-high vacuums as low as 10^{-10} mm Hg are impossible to achieve in large vacuum chambers, it goes without saying that the design becomes exceedingly more complicated and costly as the vacuum requirement progresses from 10^{-5} on down. A major design complication arises around 10^{-7} to 10^{-8} where it usually becomes necessary to provide a bake-out system. The purpose of the bake-out system is to heat the shell of the chamber under vacuum from 500°F to 700°F in order to outgas the chamber wall enough to permit attainment of the ultra-high vacuum. Elements which must be removed are gases that are adsorped on the wall surface such as H_2O and CO, as well as hydrogen which can diffuse in the bulk of the metal. The large temperature changes in the chamber wall experienced in the bake-out cycle can greatly complicate the structural design. Heating and cooling must be evenly controlled to prevent serious thermal gradients from developing.

Figure 1 illustrates the complexity imposed in the design of a large vacuum chamber by the addition of a bake-out system. This heating system consists of the circulation of Dow Therm A fluid heated by six immersion heaters. The programming of the heating rate is accomplished by means of air switches actuated by a circular chart, cam-program-recording controller. This heating system is designed to heat the

chamber to approximately 500°F within four hours. The chamber cooling system returns the chamber to ambient conditions after the bake-out, and takes approximately four hours. This cooling system has two stages of air to fluid heat exchangers and one stage of evaporative cooling. The entire control of the sequencing of these heat exchangers is automatic, requiring only energizing of the control circuit for initiation of the process.

In defining the vacuum performance specifications for a large space simulation chamber, careful attention should be given to evaluating the tradeoff between vacuum performance and the added cost and complexity of a bake-out system.

Ultra-high vacuum performance specifications may also require the added complication and cost of a double-shell wall construction. Such a construction allows for the provision of an intermediate vacuum between the inner and outer shell. This vacuum, normally referred to as a guard vacuum, is usually several orders of magnitude higher than the ultimate test vacuum. The presence of a guard vacuum minimizes the effect of leaks and imperfections which may exist on the inner wall.

2. Effects of Cold Wall and Solar Radiation System on Design of a Pressure Vessel

The subsystem interactions of a space simulation chamber also have an important effect on the design of the vacuum chamber. A major complication is the typically large number of chamber wall penetrations which are required to accommodate the cold wall and sun simulator system. Each penetration presents a structural design problem and is a potential leak

source.

Figure 2 illustrates the complexity of a space simulation facility design in terms of the large number of penetrations required. This chamber has 56 penetrations ranging in size from six inches in diameter to 48 inches in diameter. They are provided for instrumentation wires, cryogenic fluid feed-throughs, drives, solar simulation and sight ports. Personnel access is through a 5-foot door. The main access is a full-end opening door provided at the opposite end of the chamber. This pneumatically clamped door is moved six inches out from the chamber on a sliding beam and to the side on a motor-driven trolly, providing full access to the test area. All ports are sealed with double o-rings. A machine groove is provided in each plane between the o-ring grooves. This passage is provided for water cooling. The double o-ring seal also permits the introduction of a guard vacuum to this space in order to reduce seal leakage.

The cold wall can complicate the structural design of the pressure vessel by inducing thermal stresses. Figure 3 is a photograph of the inside of the chamber. The volume enclosed by the cold shroud must be large enough to house the average test specimen. Economical considerations force the size of the vacuum chamber to a minimum. Consequently, the space between the vacuum chamber wall and the cold shroud is usually small. Therefore, the cold shroud presents a significant heat sink to the vacuum chamber since it is close to the wall and is about equal in surface area. In general, the heat transfer between the wall and the cold shroud should be minimized. A typical method of limiting such heat transfer is to minimize the emissivity of the cold wall surface facing the vacuum chamber wall.

3. Effects of Operations Requirements and the Test Specimen Interactions on Design of Vacuum Chamber

The proposed use for the chamber tends to dictate it's gross volume and main access door size and orientation. Chambers now in existence include all possible door arrangements; top, bottom and side openings. Should the tank happen to be cylindrical in shape, there are differences of opinion as to whether it should be rigged horizontally or vertically.

The following series of figures show main access door configurations for three large space simulators, along with test specimen rigging techniques.

Figure 4 shows a top access location example. The entire top of the pressure chamber is removed to gain access to the test area. A jacking system lifts the top of the tank sufficiently to clear the seal, and the top is then rolled aside on a rail track. Test specimens are then installed in the chamber as shown in the photograph. In this structural design, both the main access door and the chamber are designed independently to withstand the pressure load.

Figure 5 shows a side access door configuration in a partially withdrawn position. Figure 6 is a front view of the same facility with door withdrawn and a spacecraft rigged in test position. This 15 by 25-foot door, probably the most unusual structural feature of this vacuum chamber, is designed to be a simple removable section of the chamber wall. Wedges located every three feet around the periphery of the door are engaged by hydraulic jacks and locked in place when the door is closed. Thus, the door becomes an integral structural member of the vacuum chamber. Without

the door in place, the chamber cannot withstand the compression loads. Figure 7 shows a schematic of the wedge connecting the door to the chamber mechanically and the o-ring pressure seal. The o-ring seal is compressed by members which are relatively flexible as compared to the basic structure of the tank. Hydraulically operated arms located every two feet around the door press the mating parts of the door seal together. Although two o-rings were used initially, a recent change to a one-piece extruded seal has demonstrated a greater operational tolerance to variations in seal clamping pressure during day-to-day operation.

Figure 8 shows a bottom access door configuration. It is actuated by means of jacks which raise the door to the closed position. When the door is lowered to the open position, the test specimen can be mounted on the door with good access availability. As in the case of the top access configuration, both the pressure vessel and the door are designed to withstand the pressure load independently.

At present, all three of these main door configurations are performing satisfactorily for both the mechanical and vacuum sealing functions.

Figure 9 shows a schematic outline of nine large space simulator tank configurations which have been fabricated. The top row illustrates the top access scheme. In general, large tanks such as these are braced externally in order to keep the inside surface as clean and free from bracketry as possible to minimize the outgassing problem. The left and center chambers are cylindrical tanks rigged in the vertical position. The two tanks on the lower left are cylinders which are rigged horizontally and the main access doors are located on one end of the tanks. This configuration, while considered good from the standpoint of ease of access

and test specimen handling, is incompatible with the sun simulator system designs for three of the chambers shown (i.e., the 33½ x 58-foot, the 32 x 54-foot, and the 27 x 53-foot). One of the reasons for this incompatibility is quite interesting in that it's origin is the operating characteristics of the short arc bulbs which are used in all of these sun simulator systems. To illustrate this point, Figure 10 shows a 2.5 KW HgXe short arc lamp which is used in the JPL sun simulator system. In order to maintain a reasonable life for this type of lamp, it is necessary to operate the lamp in a vertical position. It has been found experimentally that when the lamps are burned in a horizontal position, electrode material deposits on the quartz envelope above the arc and darkens an area. The resulting increase in emissivity apparently causes thermal stress large enough to fracture the envelope or degrade the performance to an unacceptable level. Therefore, the lamps are positioned vertically in each of the three large systems referenced above.

Figure 11 is a filtered picture of the arc burning in vertical operation. Figure 12 shows the polar distribution of the arc intensity with respect to the electrode centerline. It can be seen by examining the polar characteristics that more arc energy can be captured by placing the centerline of the lamp and electrode coincident with the optical beam centerline rather than normal to it. Figure 13 illustrates this point by showing that the energy in the top half of the polar is intercepted by the main parabolic reflector and is reflected around the bottom electrode and mounting structure. The bottom half of the polar is reflected back through the arc from the hemispherical cup reflector and follows the same path as the top half. If the

lamp were rotated 90° in this assembly, a portion of the beam would be blanked by the spherical cup reflector and both top and bottom electrode assemblies would interrupt the beam.

In summary, since the bulbs should be operated in an upright position and the reflected beam from the first reflector should be parallel to the bulb centerline, the centerline of the beam becomes normal to the Earth's surface. This requirement, coupled with the optical systems which were used in the three large systems in Figure 9, undoubtedly had a large influence in the selection of the vertical cylindrical tank orientation. In each case, it would have been necessary to include at least one more optical element in the system to produce a horizontal tank solar radiation beam, or to take the penalty at the lamp source described above.

The two tanks on the lower right illustrate the side opening door on a vertical cylinder scheme. This configuration combines both the ease of access and compatibility with vertical lamp mounting constraint mentioned above.

III. VACUUM CHAMBER PUMPING SYSTEM DESIGN

1. Effects of Vacuum Performance Specification on Pumping System Design

The function of the pumping system is to produce the required test vacuum in a reasonable length of time and to maintain that vacuum level for the duration of the test. A major controlling factor in the selection of a pumping system is the ultimate vacuum level desired.

Note: It was assumed that the pumping system sensitivity to vacuum level was discussed in the chapter entitled "Space Chamber Pumping Equipment", therefore, the subject is not included in this chapter.

2. Effects of Outgassing on Pumping System Design

The outgassing from the walls of the vacuum chamber, the cold wall, and the internal optical elements is an important factor contributing to the sizing of the pumping system. In the selection of materials, the designer must seek optimum combinations of strength, cost and resistance to corrosion and gas diffusivity and absorption. Stainless steel sanded and polished on the vacuum side is used extensively for the vacuum chamber construction. Both stainless steel and aluminum are used extensively in the construction of cold walls.

The characteristics of the test specimen are also of prime importance. The simulator designer in general has little control over the outgassing rates of various test specimens.

A reasonable outgassing design level should be established at the onset of the design to insure adequate capacity in the pumping system to handle the average test specimen gas load and the estimated load from other surfaces exposed to vacuum.

3. Effects of Penetrations and Seal Configuration on Pumping System

Proper design in the fabrication of penetrations and seal configurations are of prime importance and demand a great deal of attention on the part of the designer. One of the typical problems that plague the space chamber operators is the failure of seals which continually need to be maintained and replaced. There are two general classes of seals which are used in the design of high-vacuum systems:

(1) Plastically Deformed (Soft-Metal Type)

(2) Elastically Deformed (Elastomer-Type)

Figure 14 shows a schematic diagram of a typical soft-metal type seal. To effect an adequate seal using a metallic sealant or o-ring, the material must be plastically deformed by the use of relatively high forces. In order to exert the required force, heavy flanges and clamps (or bolts) must be used. The surfaces of the flanges in contact with the sealant must have close tolerances (often to within a few thousandths of an inch), and must be uniformly parallel. The metal o-ring can be used only once in most cases. If the seal is subjected to large changes in temperature, it is quite likely that the relative expansion and contraction rates of the clamp and flange combination will be out of phase. This usually results in the sealant being deformed beyond it's initial state during some point in the heating and cooling cycle. Consequently, after temperature equilibrium is reached, a leak will develop. In general, soft metal seals should be used on flanges of small diameter and only if the temperature at the seal does not vary more than a few degrees.

Figure 15 shows a schematic of an elastically deformed rubber-type o-ring

seal. In this design, the gasket or o-ring is only elastically deformed. The force required to effect a good seal is less than for the metal seal, and hence much lighter flange construction can be used. The sealant material cannot damage the flange surface, as is often the case with the soft metal seal. Under normal circumstances, the seal can be opened and closed a number of times without damage to the sealant or to the flanges. One of the important advantages of this type seal is that during thermal cycling, elastic material can conform to the changes that occur in the flange-bolt-sealant configuration. This eliminates many of the difficulties encountered with the inelastic metal sealants during heating and cooling. There are several problems, however, inherent with elastomer-type o-rings:

(1) All the elastomer components have relatively high gas permeability coefficients.

(2) Temperature range in which an elastomer composition can be used is more limited than for the metal-type sealants.

As shown in Figure 15, the temperature problem can be solved by proper seal design. Here the cooling passages near the seal groove protect the seal from over-temperature.

Figure 16 is another example of a cooled-seal configuration. In this case, the seal must be protected from solar radiation and high quartz temperatures. The following elastomer seal materials have been used successfully as simple o-rings as well as extruded shapes:

Viton A - Dupont's flurol-elastomer. Synthetic rubber with teflon, a hard material, good for at least 400°F.

Neoprene - GN and silicones, softer type material, good oil resistance, upper temperature limit 225° to 250°F.

Buena-N - Basically butyl, 70 shore, upper temperature limit of 120°F, cannot be frozen, outgassing rate is high unless completely cured.

In general, elastomer-type seal should be utilized for all the demountable components such as flanges, windows, doors, and for diffusion pump connections. It has often been found that the use of the double o-ring seal, where the space between o-rings is evacuated, does not materially improve the seal reliability.

It is extremely important to recognize that, regardless of the pumping capacity of the system, the facility in all probability will not produce the design vacuum level unless the seals are properly designed and fabricated. Leaks to atmosphere simply cannot be tolerated.

4. Fabrication Techniques - Effect on Pumping System

Strict attention must be paid toward establishing fabrication techniques including welding and cleanliness specifications. A great deal of time and effort has been lost in repairing errors of this nature. Figure 17 shows a typical combination of structural and vacuum seal welds. Before welding, the area to be welded will be cleaned with a solvent such as trichlorethyline until the surfaces are totally free from any oil or grease. Welders will be required to wear clean oil-free gloves. Upon completion of the welding, all weld surfaces exposed to high-vacuum should be ground to remove all metal convolutions or surface irregularities. Stiffeners and support brackets covering a vacuum-exposed weld should be stitch-welded to permit leak checking of the vacuum weld. In practice, it has been found valuable

to vacuum-qualify welders before committing them to work on the facility fabrications. Simple tests can be devised and the welder can practice on sample parts until he has achieved the required degree of proficiency. It should be reemphasized that the structural welds should be stitched so that leaks in the vacuum seal welds can be located. If the structural weld was continuous and leak tight, and the seal weld faulty, the joint can become a slow virtual leak and could significantly increase the pumpdown time.

5. Diffusion Pump Versus Cryogenic Pumping Tradeoff Considerations

Once having determined the magnitude of the gas load to be expected under operating conditions, the designer may elect to evaluate a tradeoff between diffusion pumps versus cryo panels, or a combination thereof. (Note: It has been assumed that the basic operating characteristics of the two different pumping systems will be discussed in the chapter entitled "Space Chamber Pumping Equipment", therefore the subject is not included in this chapter.)

Figure 18 shows various possible cryo-panel configurations. The performance is greatly influenced by detailed dimensions, and these are not optimized in the sketches. In comparing designs, several factors should be considered. These include:

1) Pumping speed;
2) Fraction of the incident energy reflected or otherwise transmitted to the 20°K surfaces (heat should be absorped by the 100°K surfaces, rather than by those at 20°K);
3) Fractions of the incident energy and gas molecules reflected toward the test item;

and,

4) Cost, etc.

Numerical evaluation of various configurations and optimization of

dimensions is a fairly complicated process. However, the following qualitative observations regarding the three typical configurations sketched in Figure 18 can be made more or less from inspection:

1) Configuration A should have a relatively high pumping speed, but also a relatively high heat load into the 20°K panels is the result of direct reflection from 100°K panels.

2) Configuration B would have a poorer pumping capability than Configuration A, but also a lower heat load into the 20°K panels.

3) Configuration C would have the lowest heat load of the three configurations since it is optically tight, however, it's pumping speed would be lower than Configuration A -- possibly comparable to Configuration B.

In summary, since vacuum specifications and outgassing rates vary widely from facility to facility, it is not possible to recommend any single combination of pumping systems as optimum. Each case must be system engineered to strike the best compromise.

IV. HEAT SINK OR COLD WALL DESIGN

The function of the cold wall or cold shroud is to simulate the heat sink of space. A major cold wall design problem is to make sure that sufficient structural compliance is built in to keep thermal stresses within nominal limits. This problem, however, is one which is fairly well understood and can be solved by using well-known cryogenic design techniques.

The surface of the wall which faces the test specimen must be flat black in color, having emissivities on the order of 0.9 to 0.95 between 0.2 and 2.7 microns (2,000 to 27,000 Å) in order to absorb most of the radiant energy from the test specimen. Any portion of the cold wall surfaces that is exposed to the direct solar radiation must also absorb this energy which is usually large compared to energy radiated and reflected from the test specimen.

Figure 19 is a photograph of a typical cold shroud. This particular shroud is a combination spacecraft mount and cold wall assembly. It was designed to roll in and out through the JPL 25-Foot Space Simulator main door opening on portable rails as a complete unit. It is fabricated of stainless steel 304 wall panels, two feet wide and 20 feet high. Each panel is composed of two stamped 16-gage sheets seam welded together to form the required LN_2 flow passages. Expansion bellows are mounted at the inlet and outlet of each panel. The inside surfaces are painted with "Sergeant Black" paint and the emissivity of the surface averages 0.85 to 0.90.

Figure 20 shows the JPL 25-Foot Space Simulator liquid nitrogen supply system. It was designed to handle from one to four tons of LN_2 per hour

depending on the amount of solar radiation energy used. The cool-down cycle for all piping and cold walls requires about 15 tons of LN_2. A 28,000-gallon LN_2 (or 100 tons) storage tank is shown in cross section in Figure 20. The cold shroud is supplied LN_2 by two pumps, a 90 GPM and a 30 GPM, the latter being used for steady-state testing conditions after the initial cool down.

As nitrogen gas is generated in the cold walls, it rises to the top header and is exhausted to atmoshpere past a low pressure relief valve. A separator upstream of the relief valve returns any LN_2 to the main storage tank.

V. SOLAR RADIATION SYSTEM DESIGN

This section will be devoted to reviewing subsystem interactions on the solar simulation system design. Specific design characteristics of various sun systems will not be included since such information is presented in another chapter of this report. It is worth emphasizing, however, that the state-of-the-art in solar simulation falls farther short of typical performance requirements than any other space simulator subsystem.

1. Effect of Solar Simulation Specification on Solar Simulation Design

The function of a solar radiation system should be to produce the same effect on the spacecraft or test specimen as the real sun. The specification usually includes an intensity level of at least one solar constant (130 watts/ft^2 at the orbital distance of the earth), reasonable uniformity across the solar beam ($\pm$ 10%), and as small a collimation angle as possible ($\pm$ 5° or less). It is also desirable to match the effect of the solar spectrum in the range from 2,000 to 40,000 Å, since most of the sun's radiant energy falls within this band width. One of the most difficult sun characteristics to achieve is a high degree of collimation. The following paragraphs describe a study undertaken to explore in some detail what level of collimation may be considered acceptable for specific application.

Certain spacecraft are more sensitive to collimation than others. For example, the JPL Mariner 3 spacecraft shown in Figure 21 flies sun-oriented and is quite sensitive to shadow pattern and excess energy falling on surfaces which are intended to be aligned with the sun's rays. In order to gain a better insight into the latter problem, a calculation was made

to determine the incident energy on sloping surfaces versus collimation in solar simulation. It was felt desirable from accurate temperature control considerations to know the difference in energy flux that a variation in collimation may produce on a given surface. The purpose of this calculation was to furnish such information in an absolute form. Figure 22 graphically presents the results of this calculation. Appendix 1 describes the calculation in detail.

The results of the calculation may be summarized as follows: 1) The difference in energy flux between the sun's collimation angle and the best state-of-the-art sun simulators is negligible if the spacecraft surface is misaligned by two degrees or more. In most cases, the spacecraft attitude control system will not position better than $\pm 1^{\circ}$. 2) The errors shown for a perfectly aligned surface, while large percentage-wise, are small in absolute magnitude when compared to the incident energy for alphas greater than two degrees.

From September to December, 1962, consistent temperature distributions of the MR 2 were obtained by telemetry enroute to Venus. In January, 1963, a Mariner 3 spacecraft of identical design to the Mariner 2 was tested in the JPL 25-Foot Space Simulator under simulated flight conditions. Figure 21 is a photograph of the Mariner 3 spacecraft mounted in test position. The solar simulation collimation half-angle was 5.2° (the real sun being $\frac{1}{4}^{\circ}$ at the Earth's orbital distance). The agreement between the flight data and the ground test was adequate to establish the ground test results as very useful emperical design data.

In light of these theoretical and experimental results, it is recommended that design tradeoff studies be carried out in order to determine as well as possible the most realistic and economical solar

simulation specification before committing to a design effort.

A controlling philosophy in the systems design of a large space simulator should be to subordinate the design of all subsystems to the solar simulation system. The solar simulation system should be engineered with a minimum of constraints imposed by the other major subsystems. Ideally, the solar radiation system should be established and the tank, cold wall, shroud panels and pumping system should be in effect wrapped around the sun system. In searching for better-collimated and more-uniform solar simulation performance, vacuum tanks will tend to become longer in the future. This prediction will be explained in detail later in this chapter.

2. Effect of Heat Sink or Cold Wall on Solar Simulator Design

In order to maintain the continuity of the cold wall facing the model, it is necessary to cool the internal optics and at the same time retain acceptable reflectivity. Figure 23 shows a segment of the JPL 25-Foot Space Simulator parabolic reflector whose internal surface faces the test specimen. From six to ten flexible battery cable type straps are used to conduct heat away from each mirror element to the cold gaseous nitrogen lines. The mirror surface does not require cooling to the extremely low temperatures of the black cold wall liners because of the low emissivity (high-reflectivity) of the mirrors in the infrared region. The basic requirement for the mirror cooling was that it would not contribute more radiation per unit area than a unit area of the black cold walls at -300°F. Radiation is directly proportional to the emissivity and to the fourth power of an absolute given temperature for a given surface. Thus, the required mirror temperature was calculated to be in the -50 to -100°F range. The calculation was based on the radiation relationship $\epsilon_w T_w^4 = \epsilon_m T_m^4$,

where " ϵ " is the emissivity of the wall and mirror, respectively, and "T" is the absolute temperature of the wall and mirror, respectively.

3. Effect of Test Specimen Solar Simulation Design

The particular characteristics of the class of test specimens to be investigated can also affect the design of the optical system, particularly in the case where the specimen has specularly reflecting surfaces. In this case, the internal optics must be arranged such that specular reflections from the model cannot re-reflect from the internal optical elements and return to the test specimen. This requirement, coupled with a quest for better collimation has induced the designer to tend toward "off-axis" optical systems.

Many solar simulator arrangements are similar to telescopes working in reverse. That is, light is collected into a small, intense bundle and injected into the system at the focal point of a parabola, which in turn reflects a large, uniform, well-collimated beam into the test volume. Figure 24 illustrates the classical Herschelian, or "off-axis" system, which seems to be the most promising arrangement for two reasons. First, no shadow or penumbra is produced by obstructing the final beam with an injection reflector, and, secondly, it is possible to arrange the system so that no energy leaving the test article and striking the parabola is reflected directly back onto the test article. The major disadvantage of this arrangement is that an off-axis paraboloid, or an approximation thereof, is required.

Solar simulators of this general class can usually be divided into two parts; the energy collection system (light sources) and the remaining

energy distribution system, such as described above. A compromise must be effected between these parts to resolve their conflicting requirements for large quantities of energy to achieve the high illumination levels desired and a point source of illumination for the parabola in order to obtain a high-degree of collimation.

The most uncollimated ray in the test volume will result from the ray making the greatest angle α (see Figure 24) to the parabola with a ray passing through the focus to the same point on the reflector. Thus, the collimation depends upon the ratio of the size of the beam at the parabola focus and it's distance from that reflector. In a given system, then, collimation can be improved by reducing the size of the injected beam or by increasing the focal length of the parabola. Since the size of the illuminating beam is determined by the amount of energy required, the practical limitations of the sources of energy and the laws of magnification, increasing the focal length is the most nearly independent variable.

Generalities such as these cannot be drawn concerning the energy collection portion of the system, since each arrangement has it's own set of parameters. It is clear, however, that benefits can be obtained by minimizing the size of the illuminating source and by increasing the reflector's focal length diameter ratio. This is the basis for the prediction which was made earlier that vacuum tanks will tend to become larger in order to accommodate longer focal length optical systems.

4. The Effect of Oil Contamination of the Internal Optics

Most space environment simulators use oil diffusion pumps in the high-vacuum pumping system. Oil migrating throughout the system and depositing on various surfaces present a problem that has not been thoroughly investigated.

In particular, a very thin film of oil might have a marked effect on the reflective and absorptive properties of sun simulator optics, cold shrouds and the test specimen. Recent experiments have been performed at JPL which indicate that it is possible to deposit a detectable film of oil on a mirror surface in an oil diffusion pumped system with LN_2 traps and a surrounding LN_2 shroud. This is evidence that an unexplored phenomena exists whose effect may be significant. At this time, however, no definitive results have been obtained and no engineering conclusions can be drawn.

The following is a brief description of these preliminary experiments. A segment of the 25-Foot Space Simulator parabolic aluminum mirror was mounted on a temperature control plate and hung inside the LN_2 shroud of a 30 by 50-inch vacuum chamber (see Figure 25). The mirror was then illuminated by a 12-inch diameter, 200 watt/ft^2 light beam produced by a Genarco carbon arc lamp and projected through a 12-inch diameter quartz window onto the mirror segment.

In all of the seven experiments, the chamber was evacuated to better than 1×10^{-6} mm Hg; the roughling line and diffusion pump cold traps and wall shrouds were filled with LN_2. Each experiment was run for nine hours with the carbon arc light on.

A slight haze of oil was detected on the mirror in the five experiments where the mirror was maintained at $0^{\circ}F$. There was no oil detected on the mirror during the two experiments where the mirror was maintained at $20^{\circ}F$.

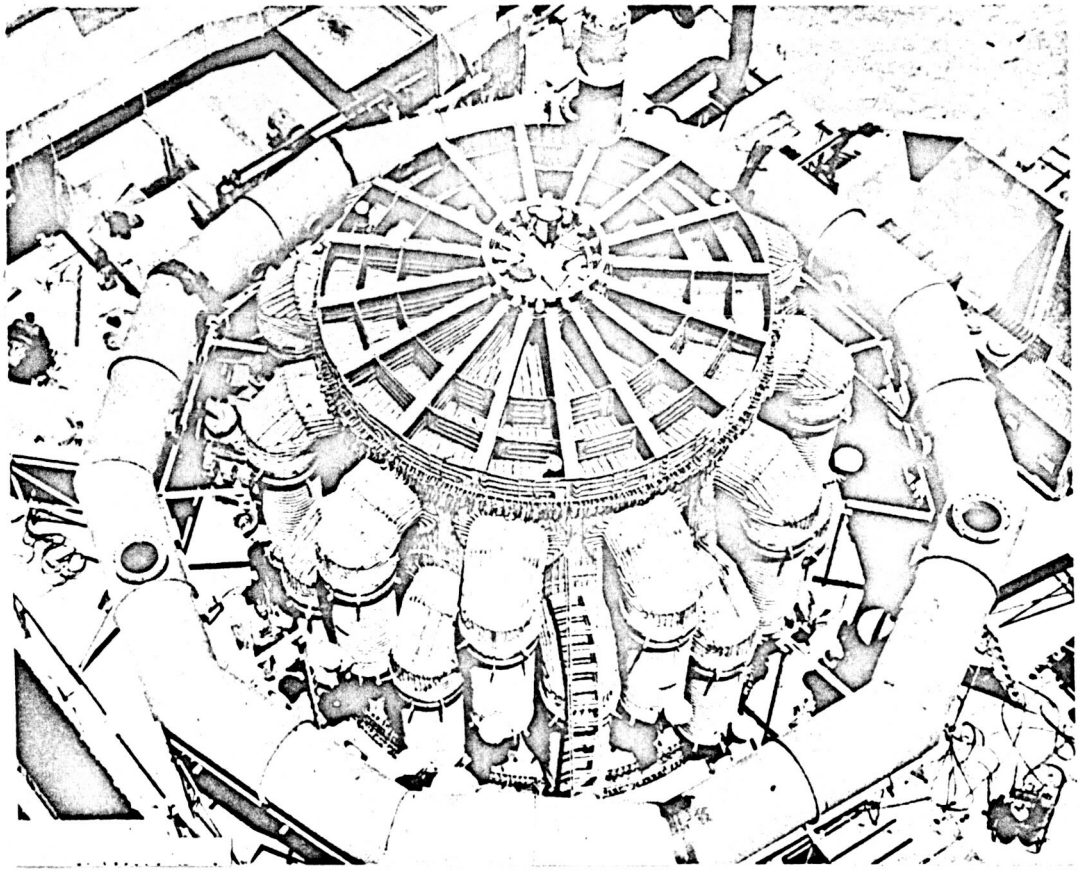

FIGURE 1. Vacuum Chamber Bake-Out System

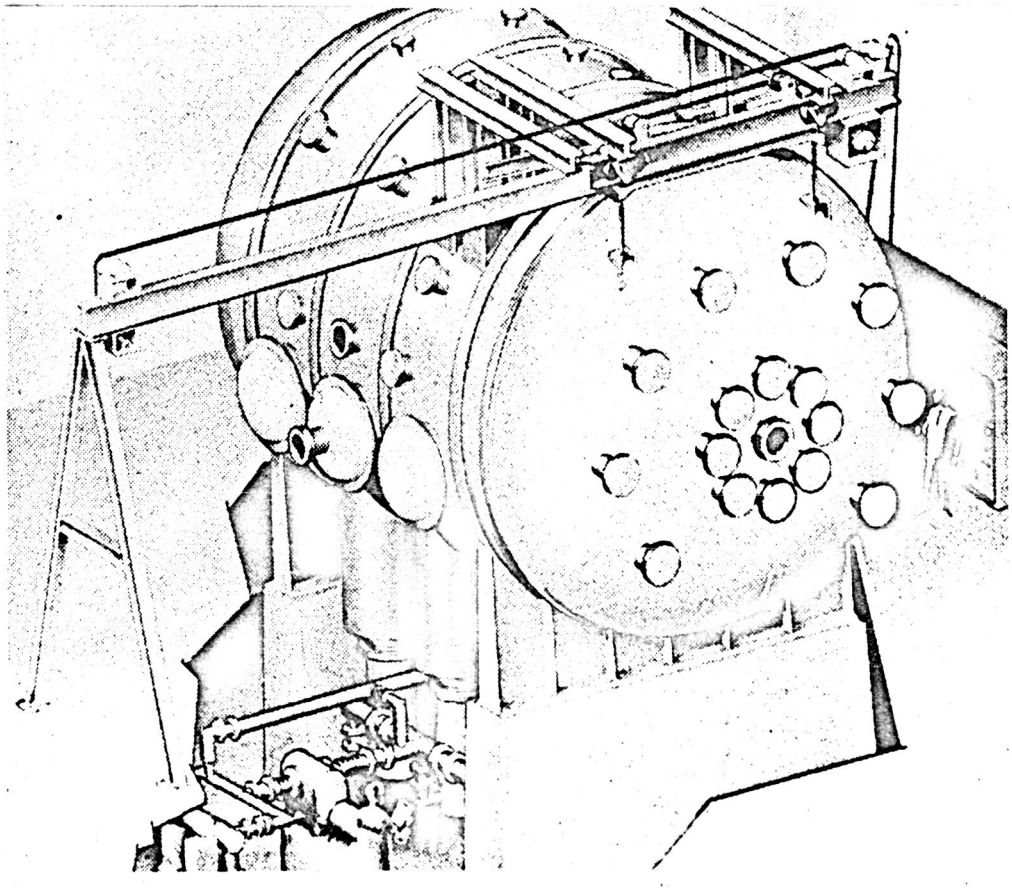

FIGURE 2. Vacuum Chamber with 56 Penetrations - Outside View

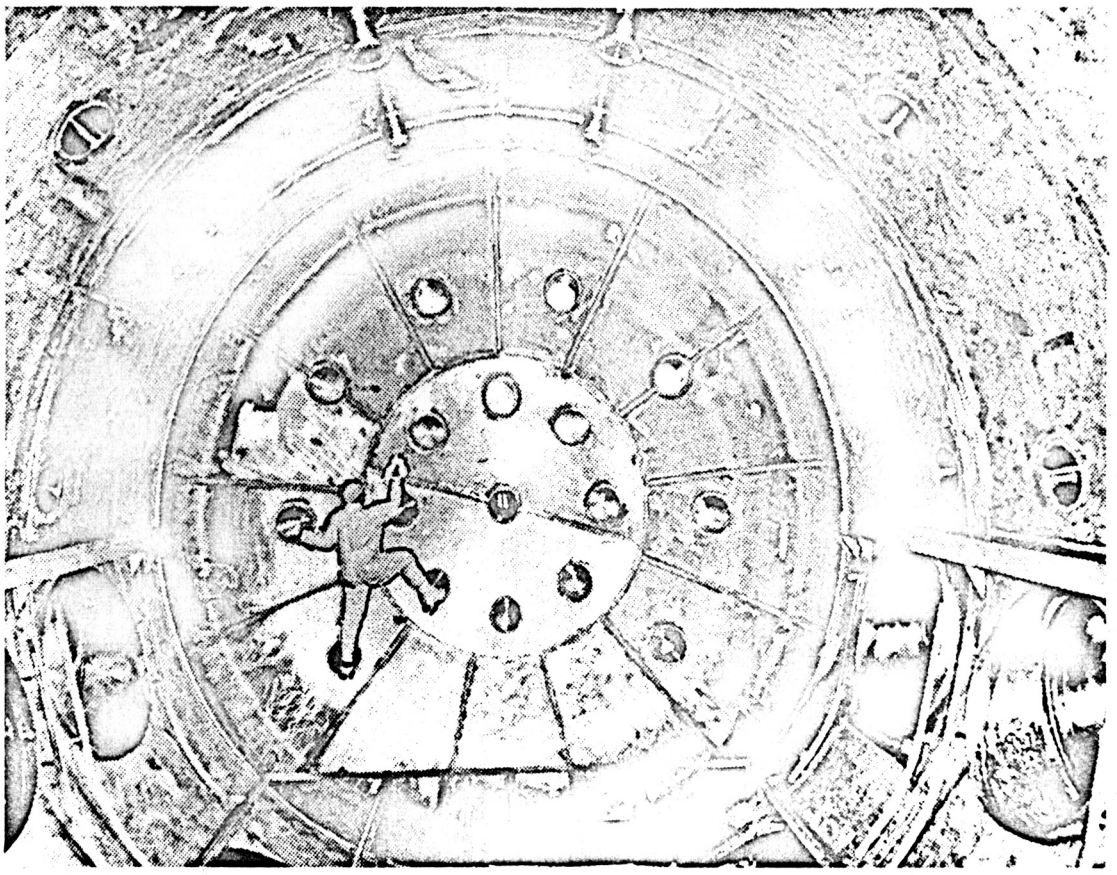

FIGURE 3. Vacuum Chamber with 56 Penetrations - Inside View

FIGURE 4. Top Access Vacuum Tank and Test Specimen

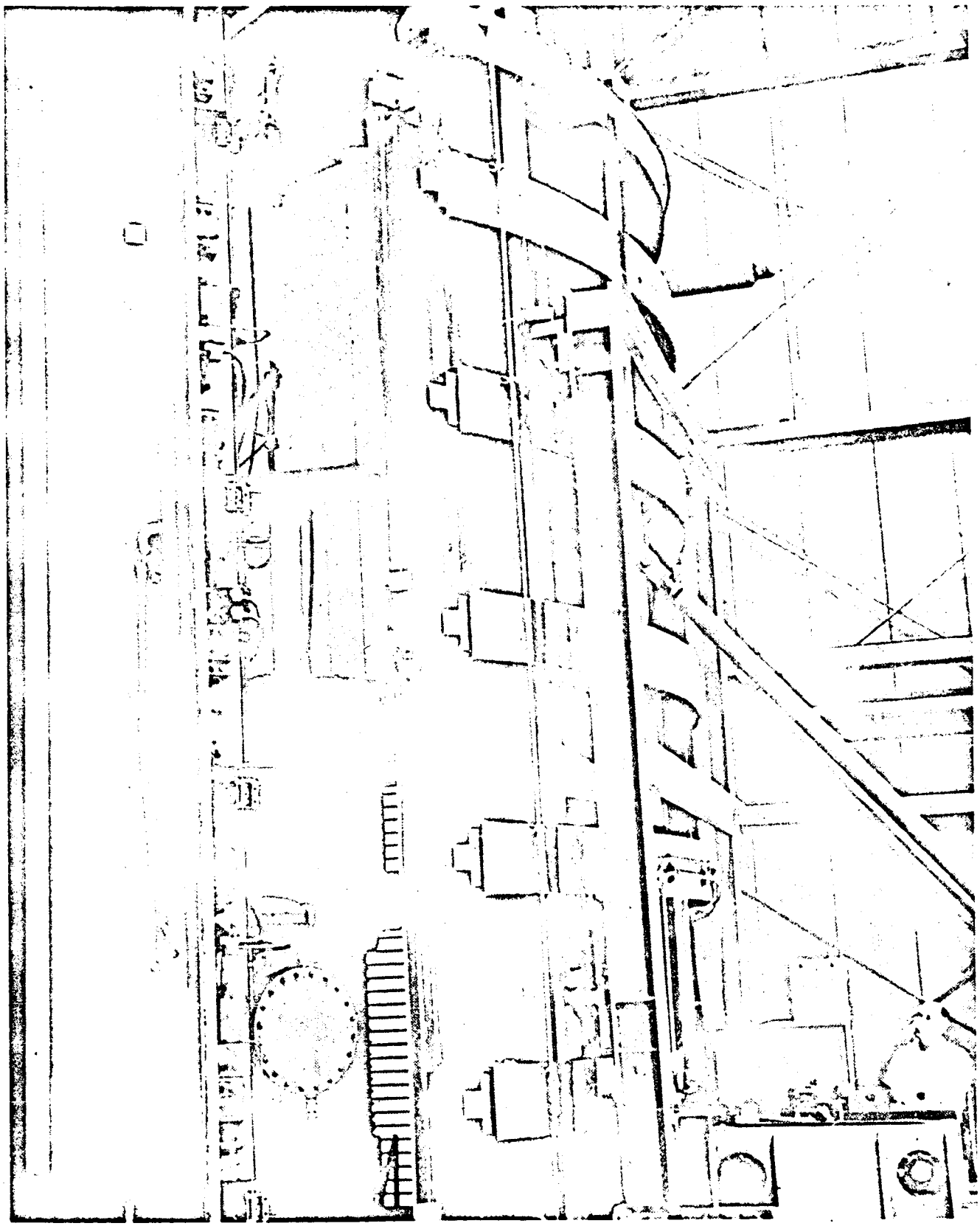

FIGURE 5. Side Access Vacuum Tank - Partly Open

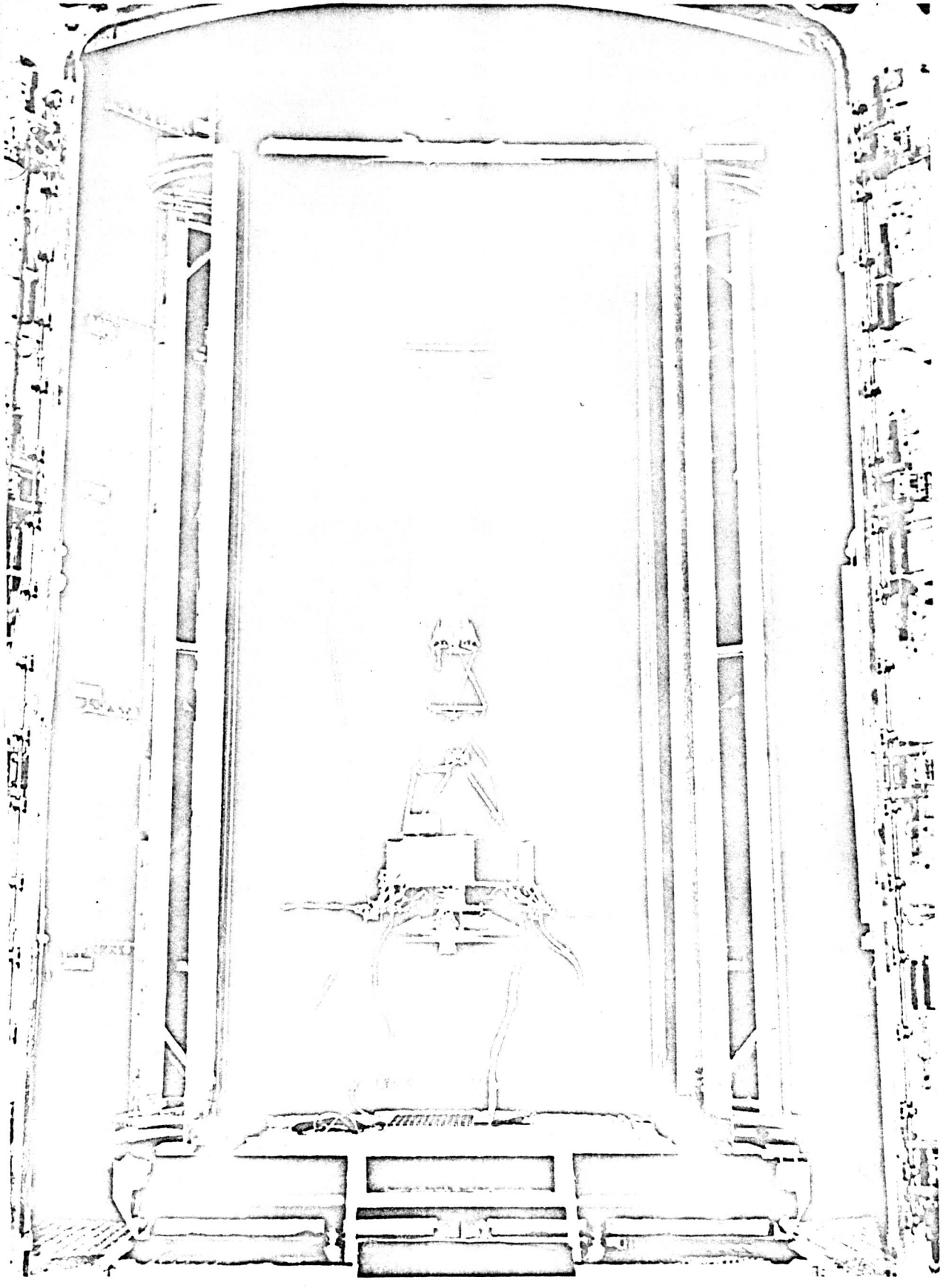

FIGURE 6. Side Access Vacuum Tank and Test Specimen

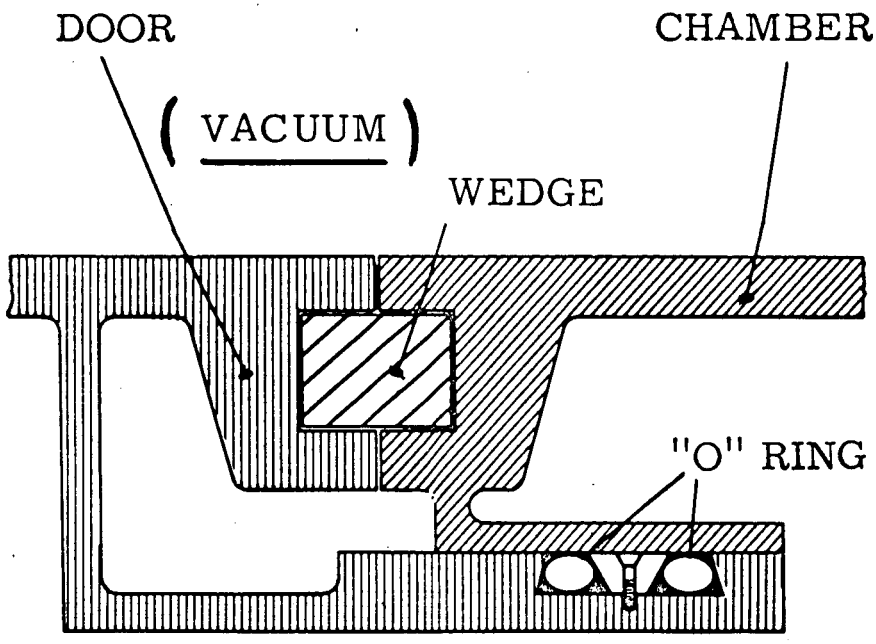

Door seal and structural locks
(schematic)

FIGURE 7. Side Access Vacuum Tank Seal and Lock Configuration

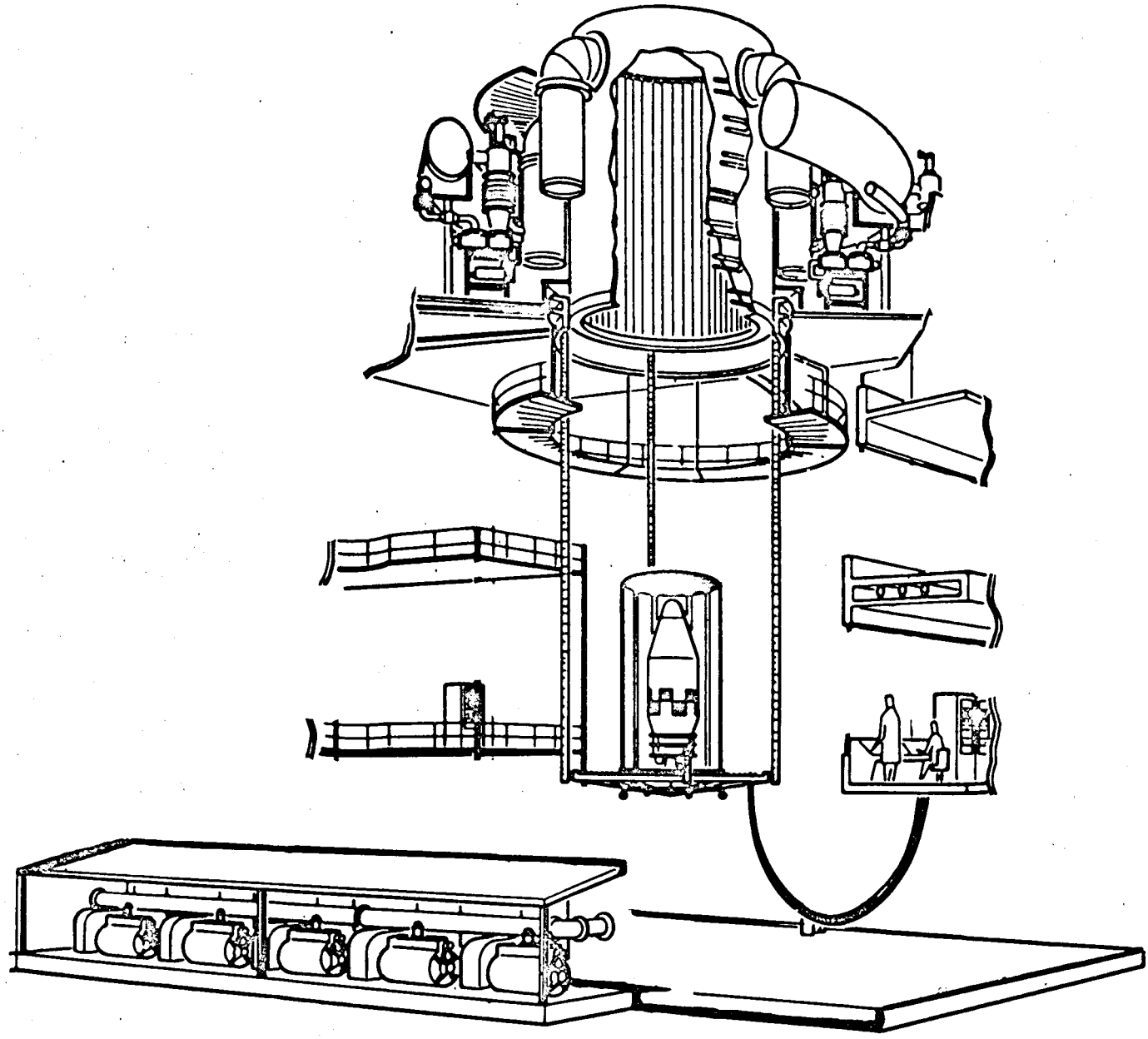

FIGURE 8. Bottom Access Vacuum Tank and Test Specimen

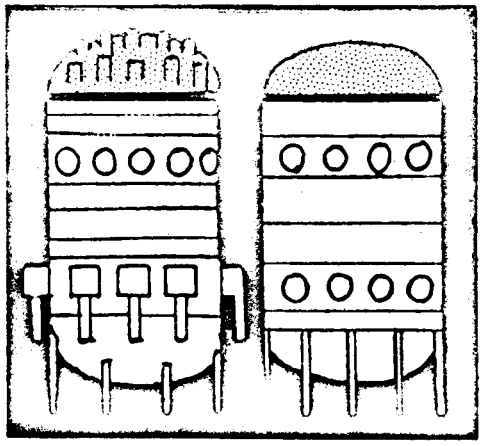

33-1/2 x 58 ft

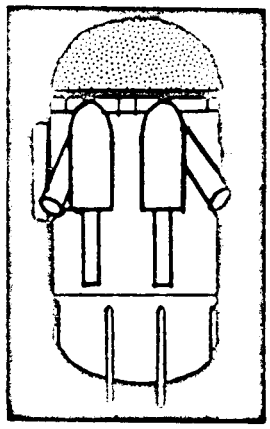

32 x 54 ft

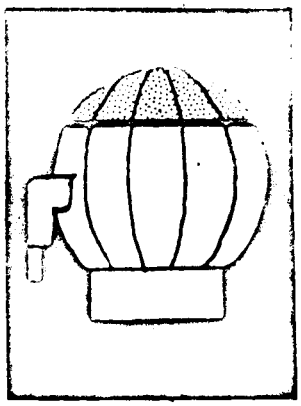

38-1/2 ft

Dotted area indicates
movable portion of simulator.

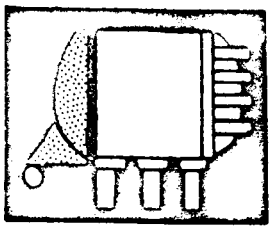

12 x 16 ft

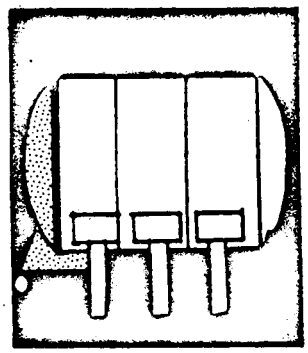

18 x 30 ft

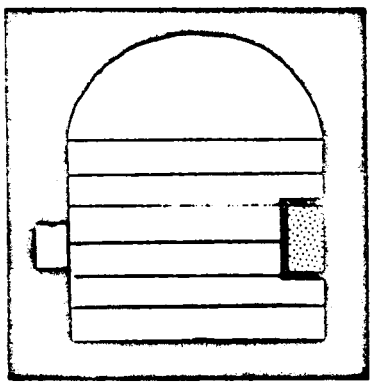

58 x 55 ft

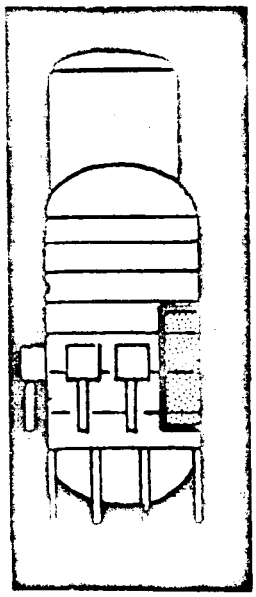

27 x 53 ft

FIGURE 9. Nine Large Vacuum Tank Configuration

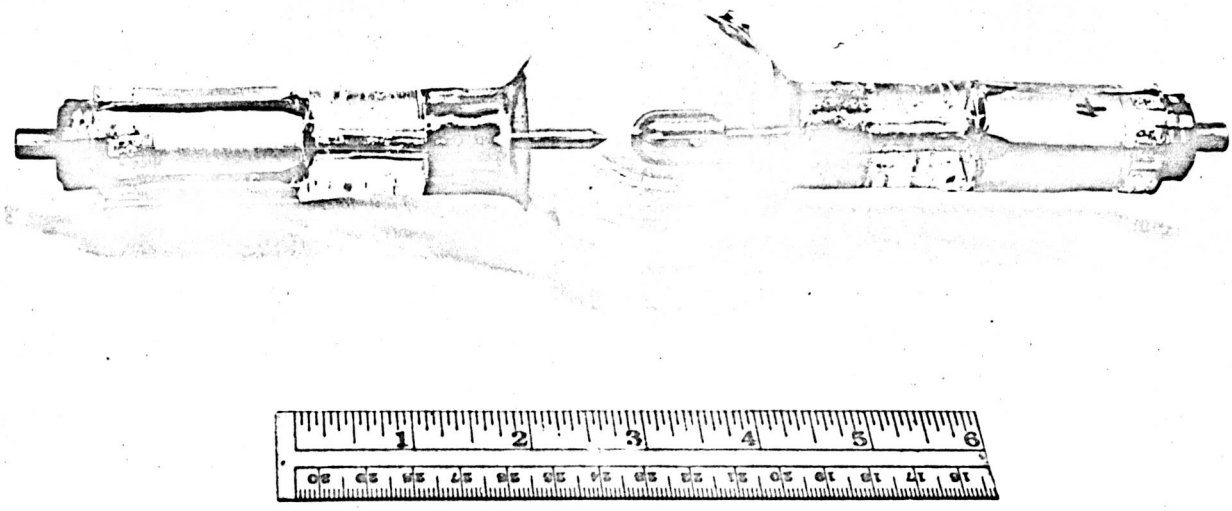

FIGURE 10. Hannovia 2.5 KW HgXe Lamp

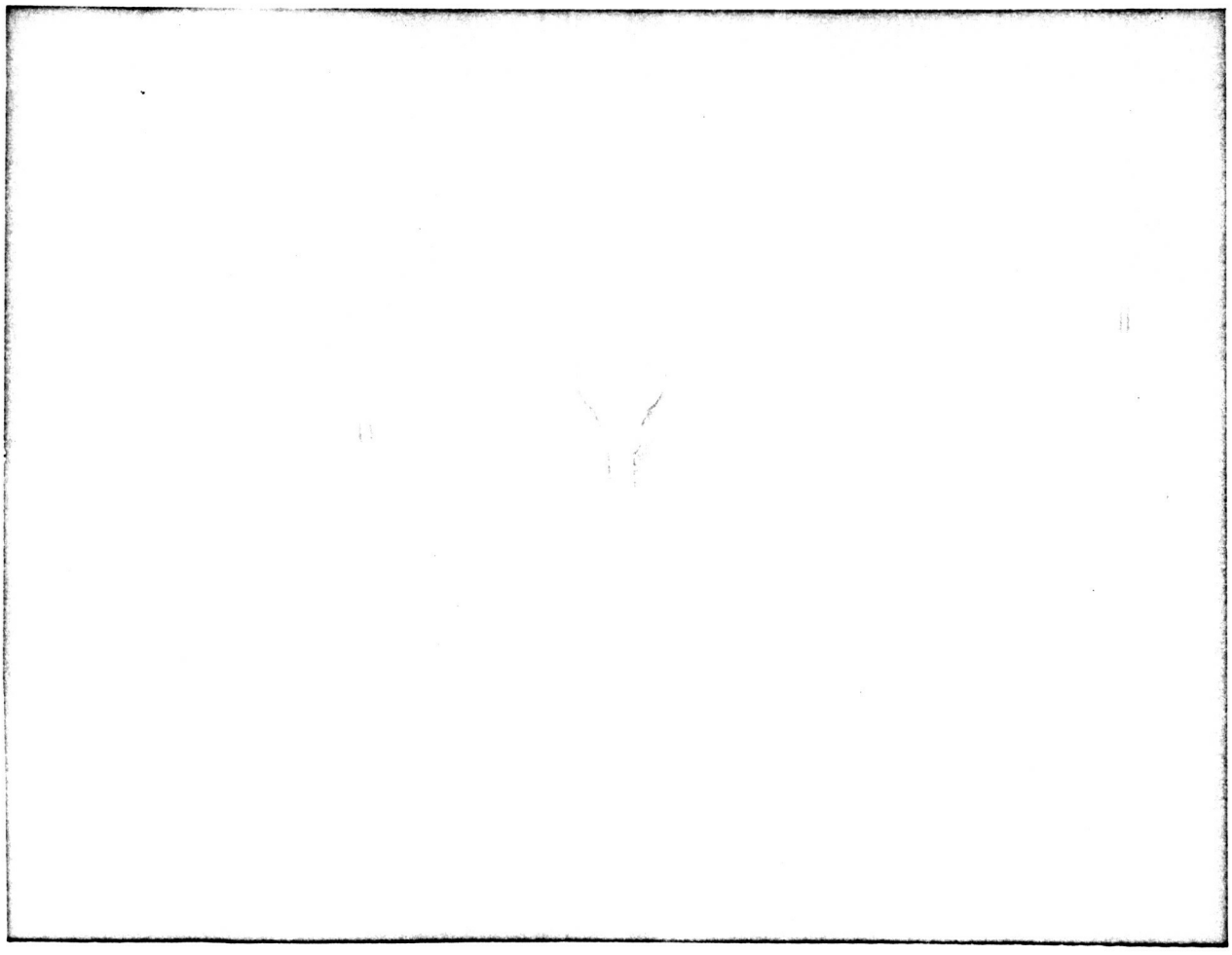

FIGURE 11. Hannovia 2.5 KW HgXe Lamp, Arc Photo

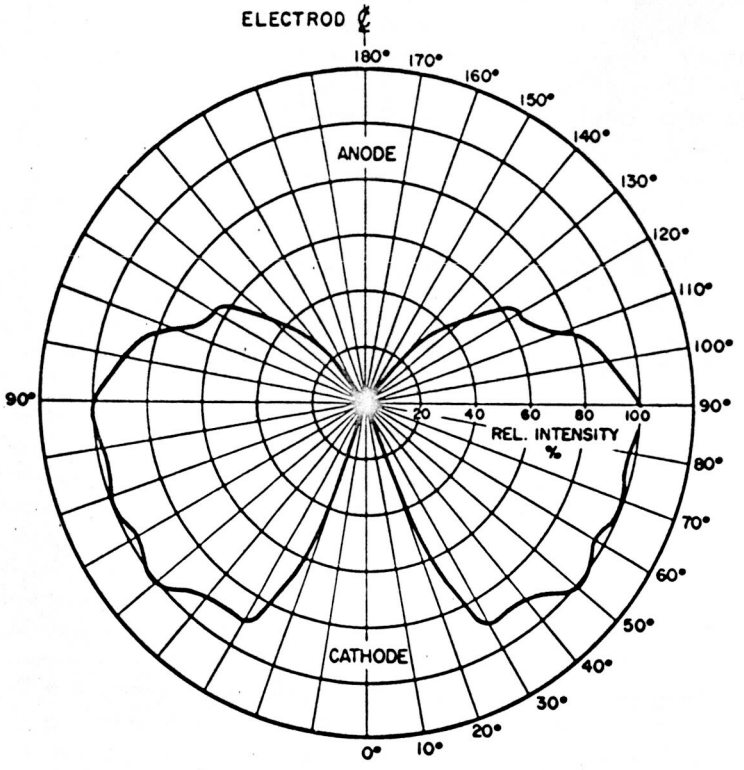

FIGURE 12. 2.5 KW HgXe Lamp, Intensity Polar

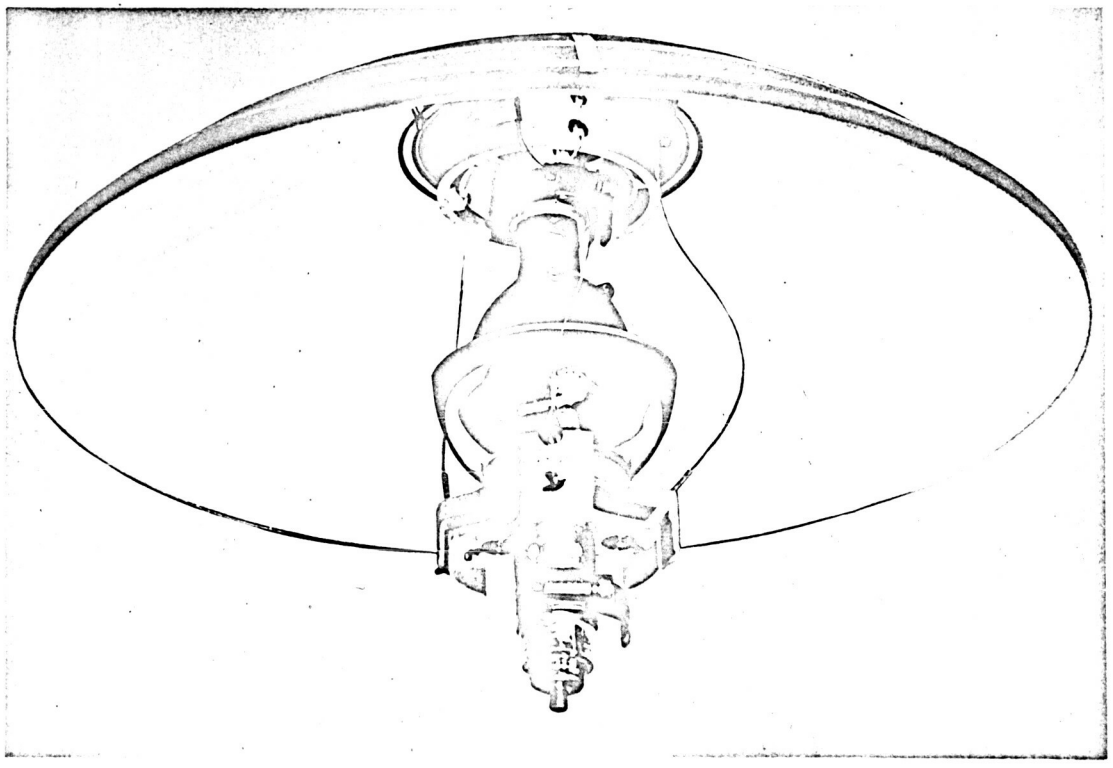

FIGURE 13. 2.5 KW JPL Reflector Assembly

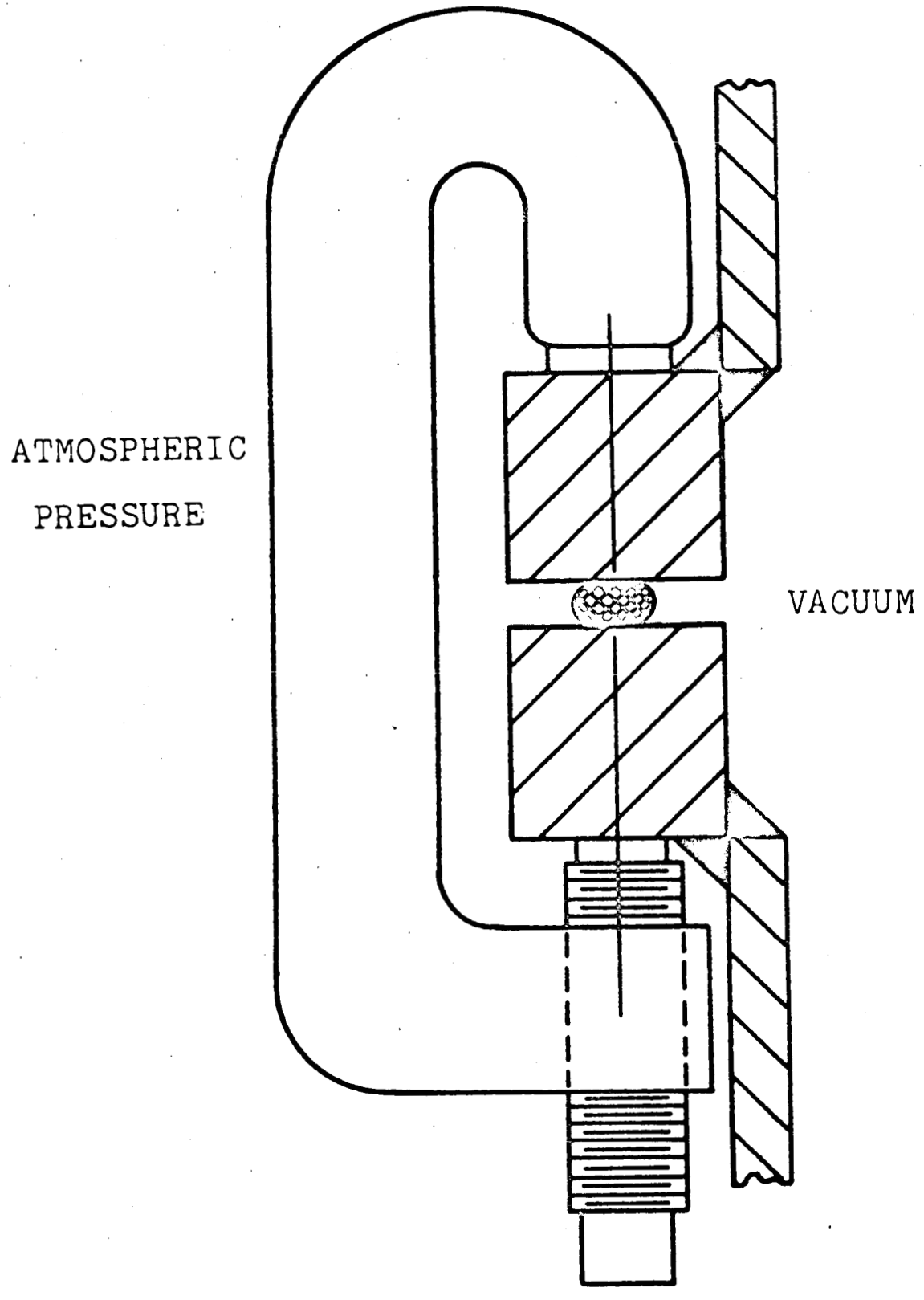

FIGURE 14. Typical Soft-Metal Seal Configuration

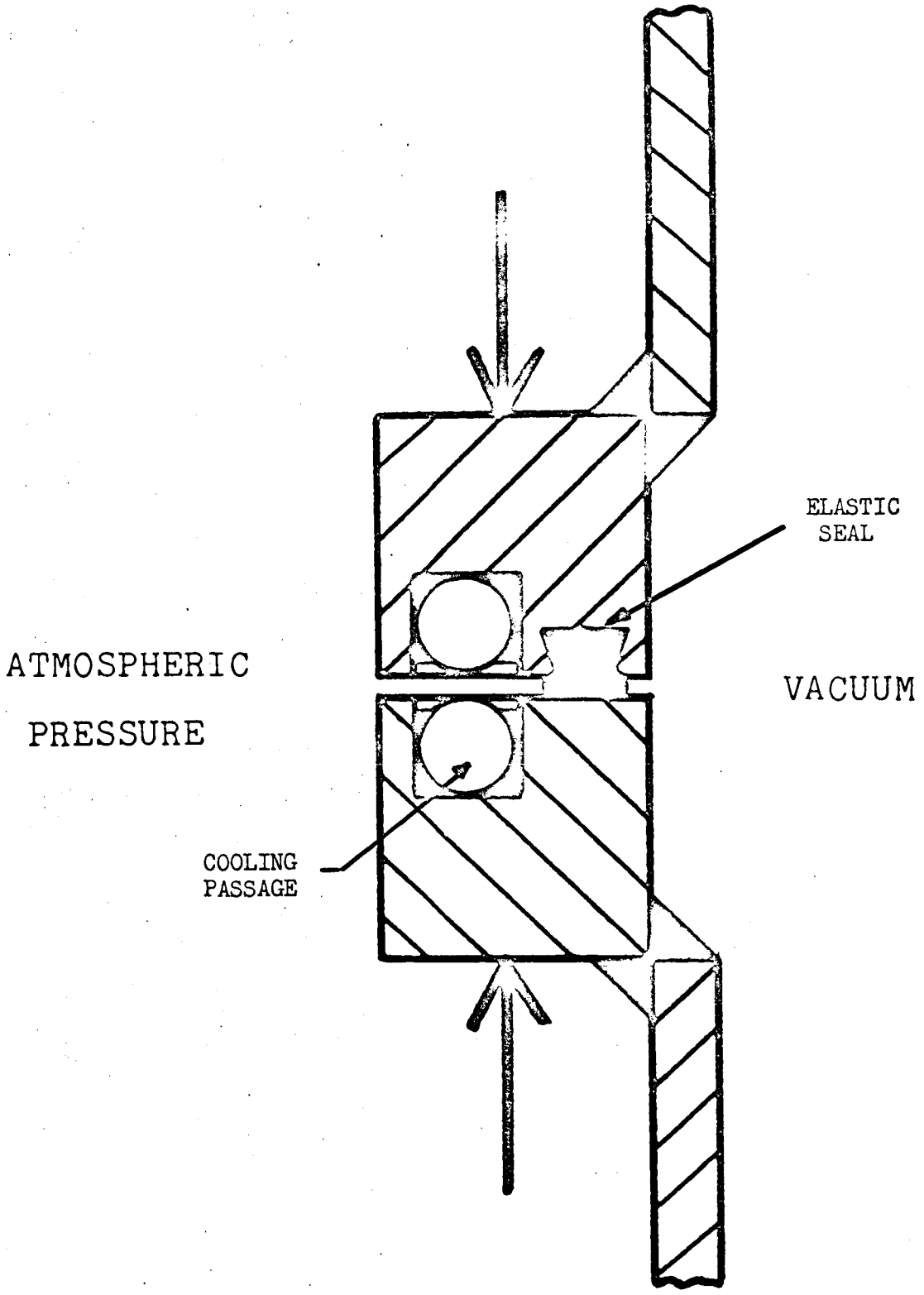

FIGURE 15. Typical Elastic Seal with Cooling System

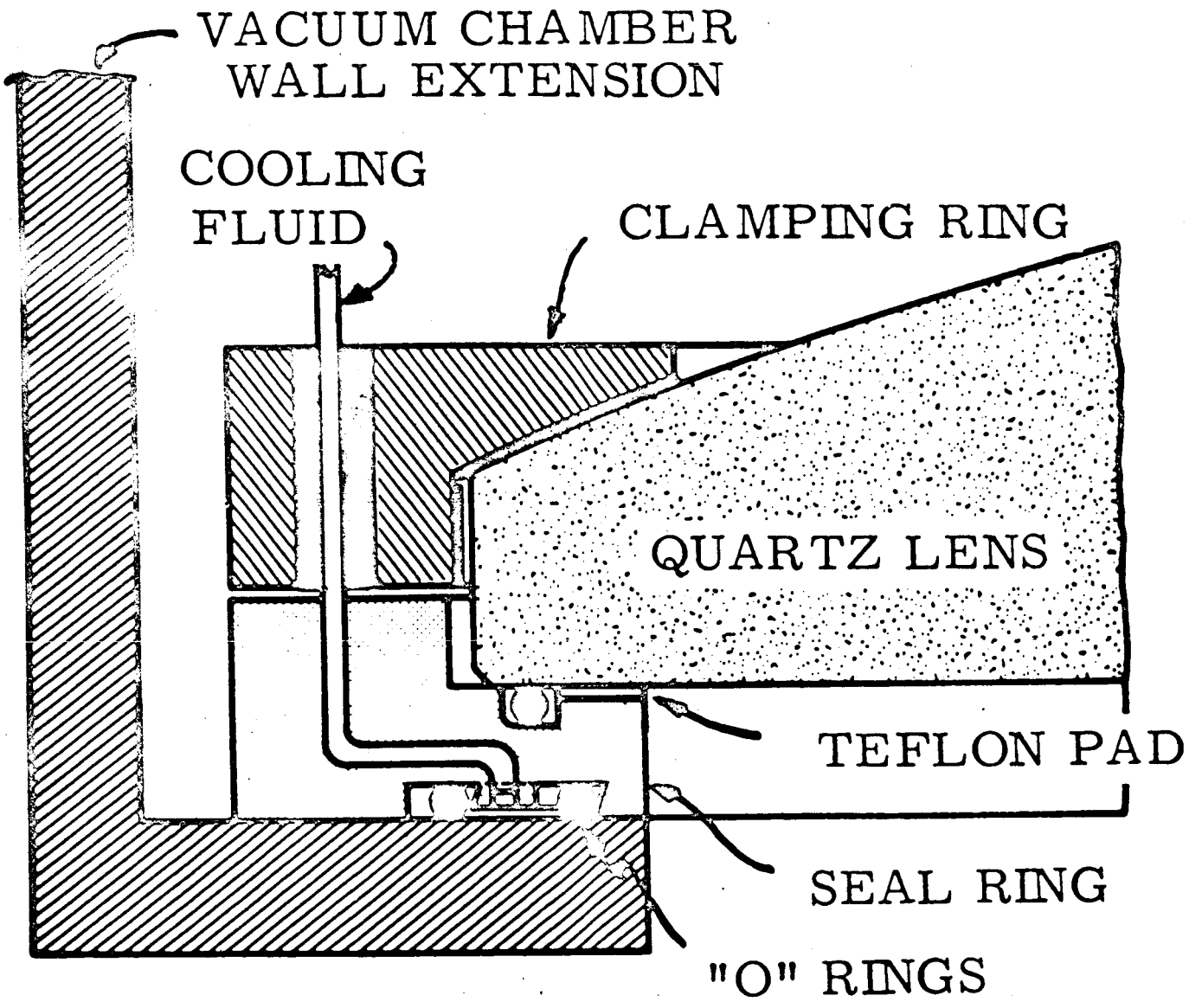

FIGURE 16. Lens Seal with Cooling

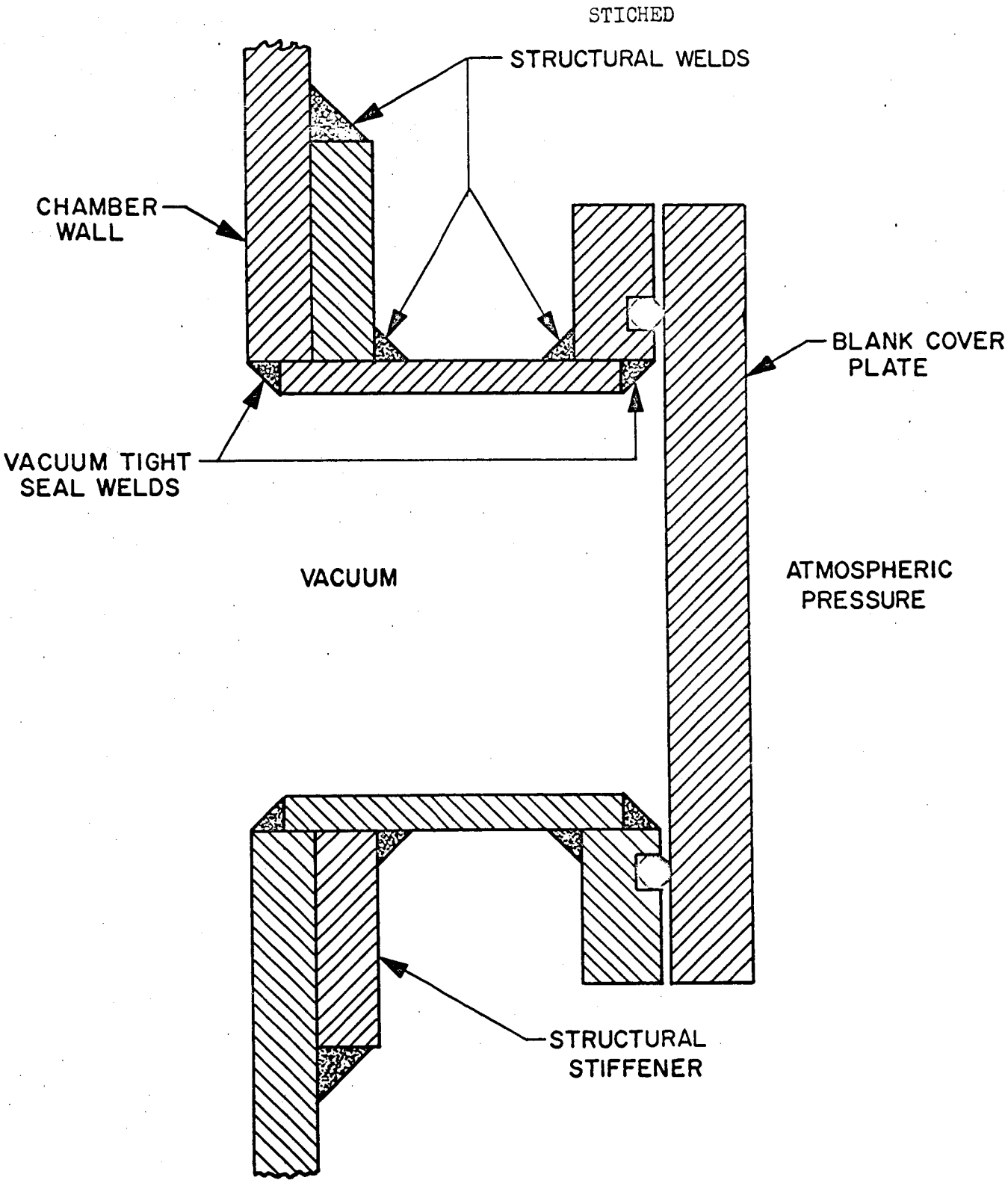

FIGURE 17. Typical Welding Configurations

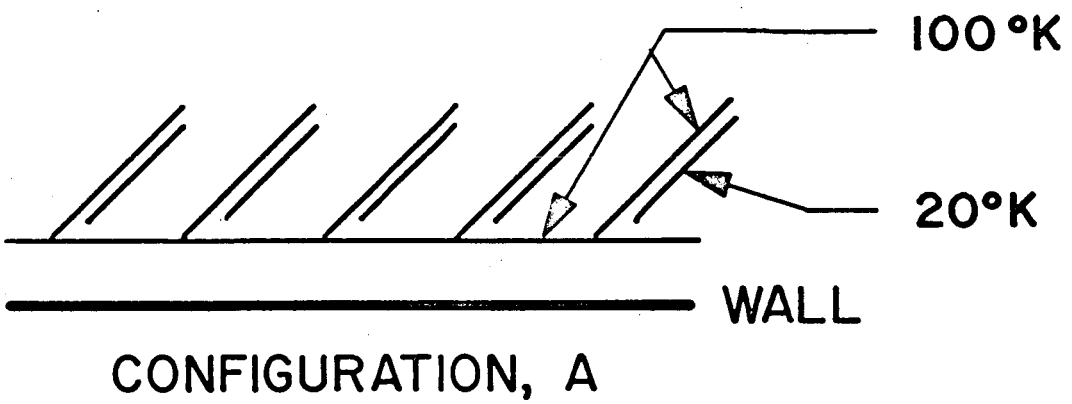

CONFIGURATION, A

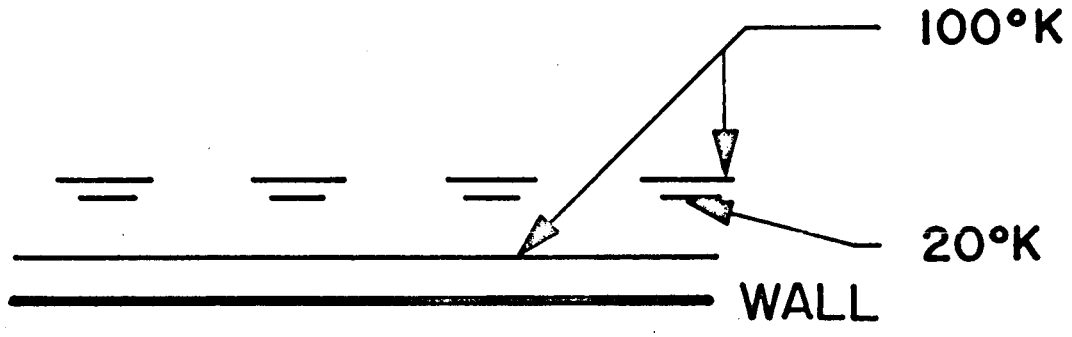

CONFIGURATION, B

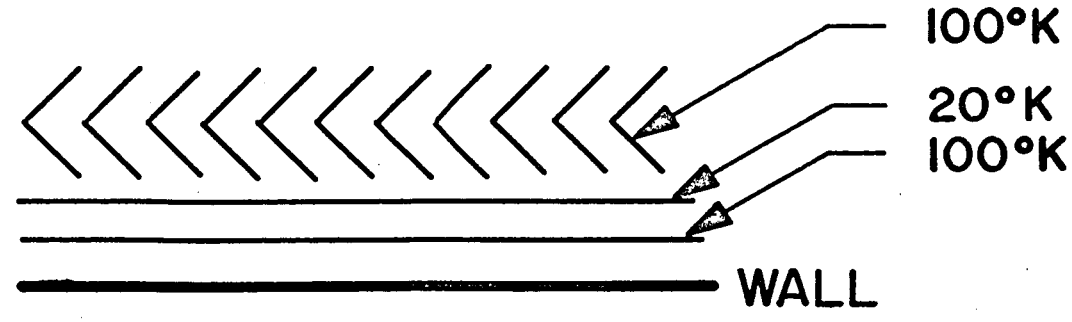

CONFIGURATION, C

FIGURE 18. Typical Cryogenic Panel Design

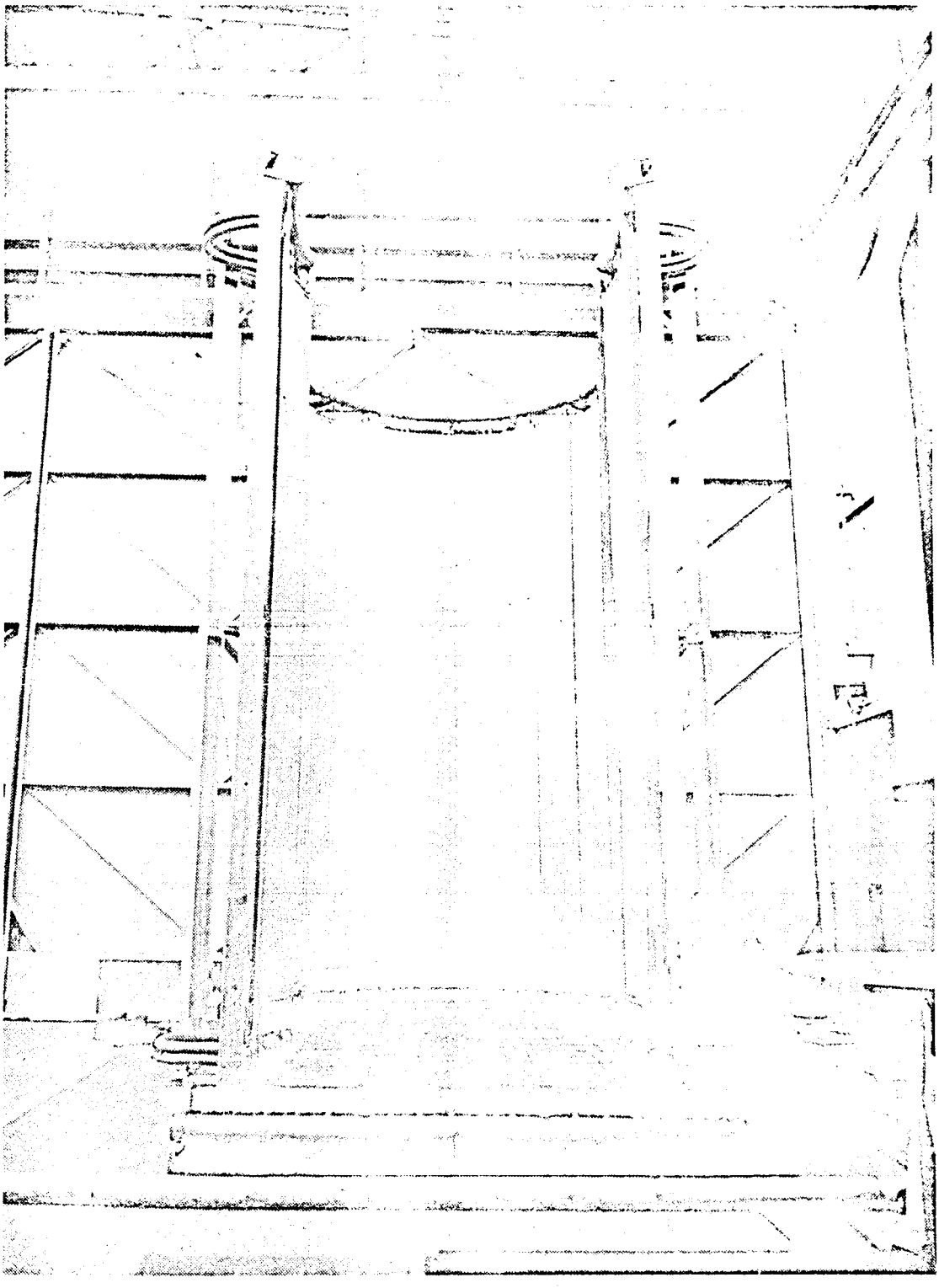

FIGURE 19. JPL Portable Cold Wall Shroud

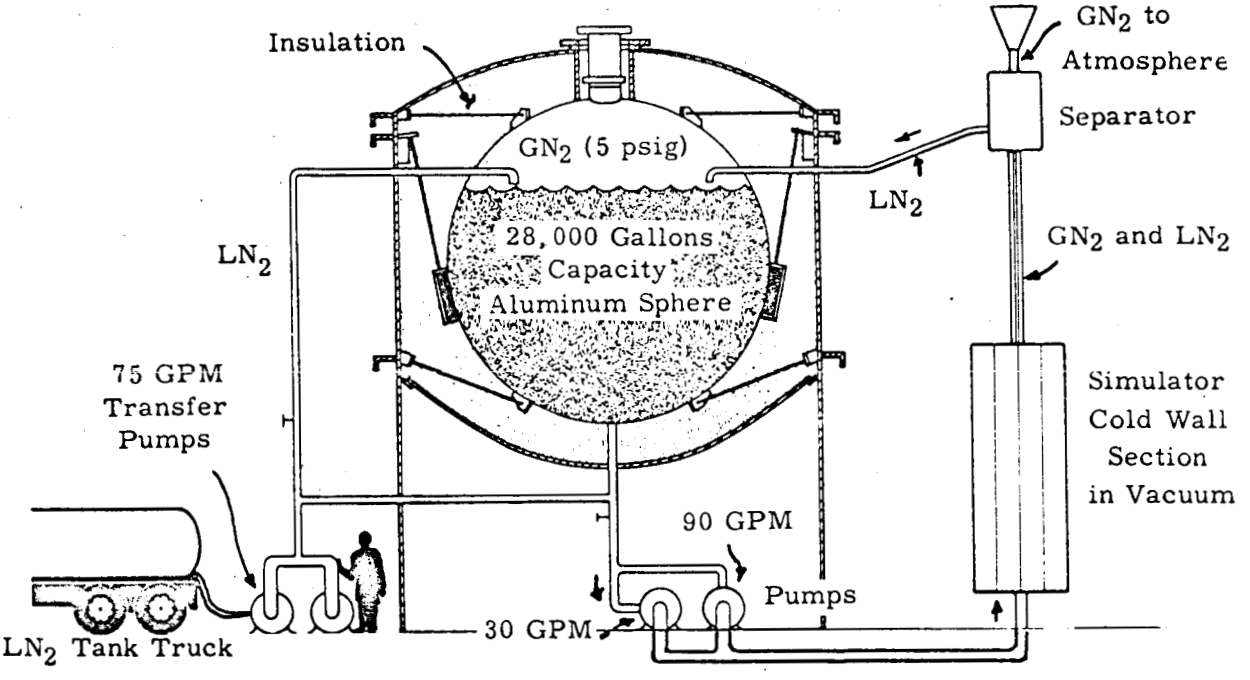

FIGURE 20. JPL LN_2 Storage Tank and System Schematic

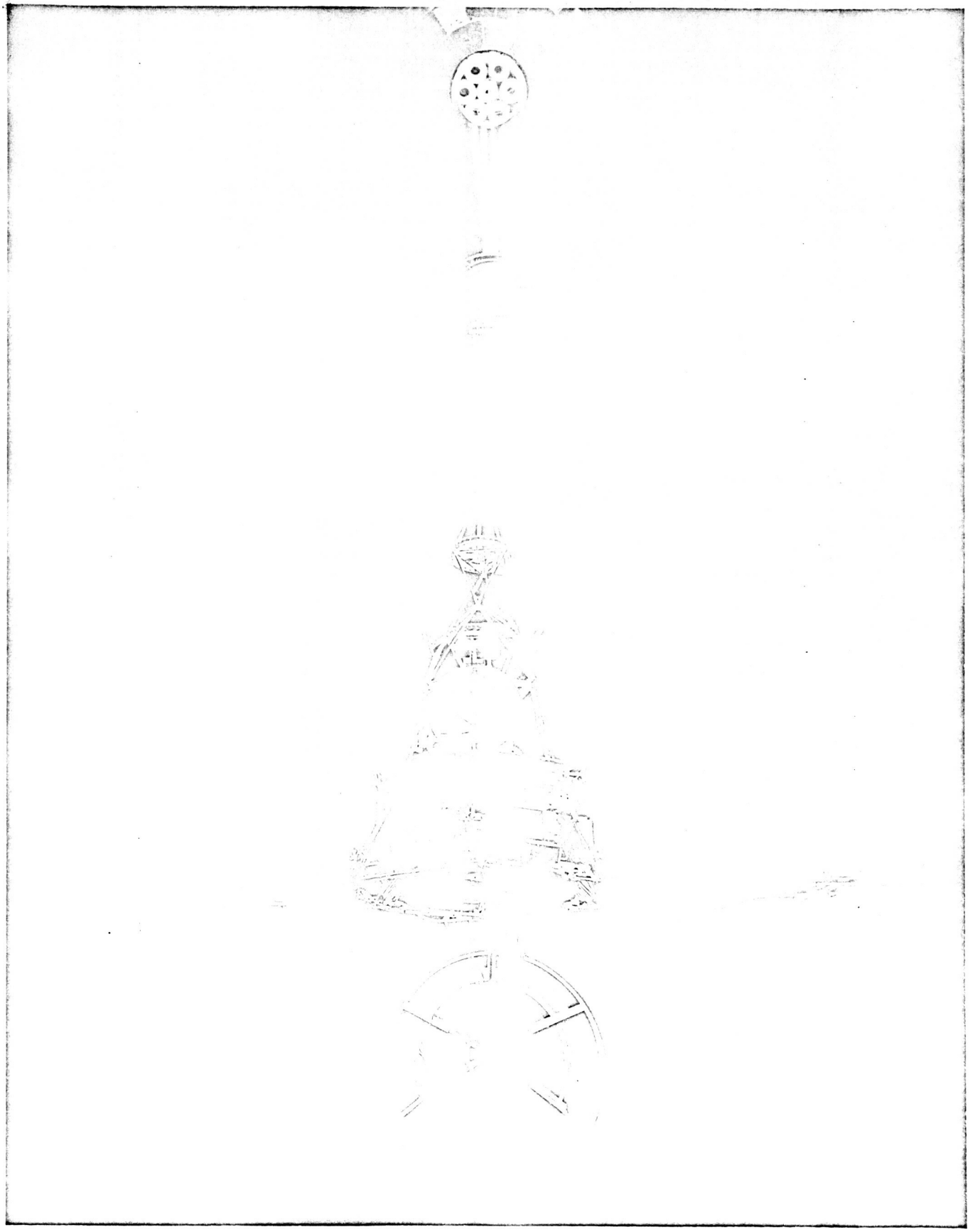

FIGURE 21. JPL Mariner 3 Spacecraft

NOTE:
1. Plane of unit area is perpendicular to plane of ecliptic
2. α is measured in plane of ecliptic
3. α is angle measured between the following:
   a. Line of intersection between unit area and ecliptic plane
   b. Line joining center of unit area to center of disc representing Sun

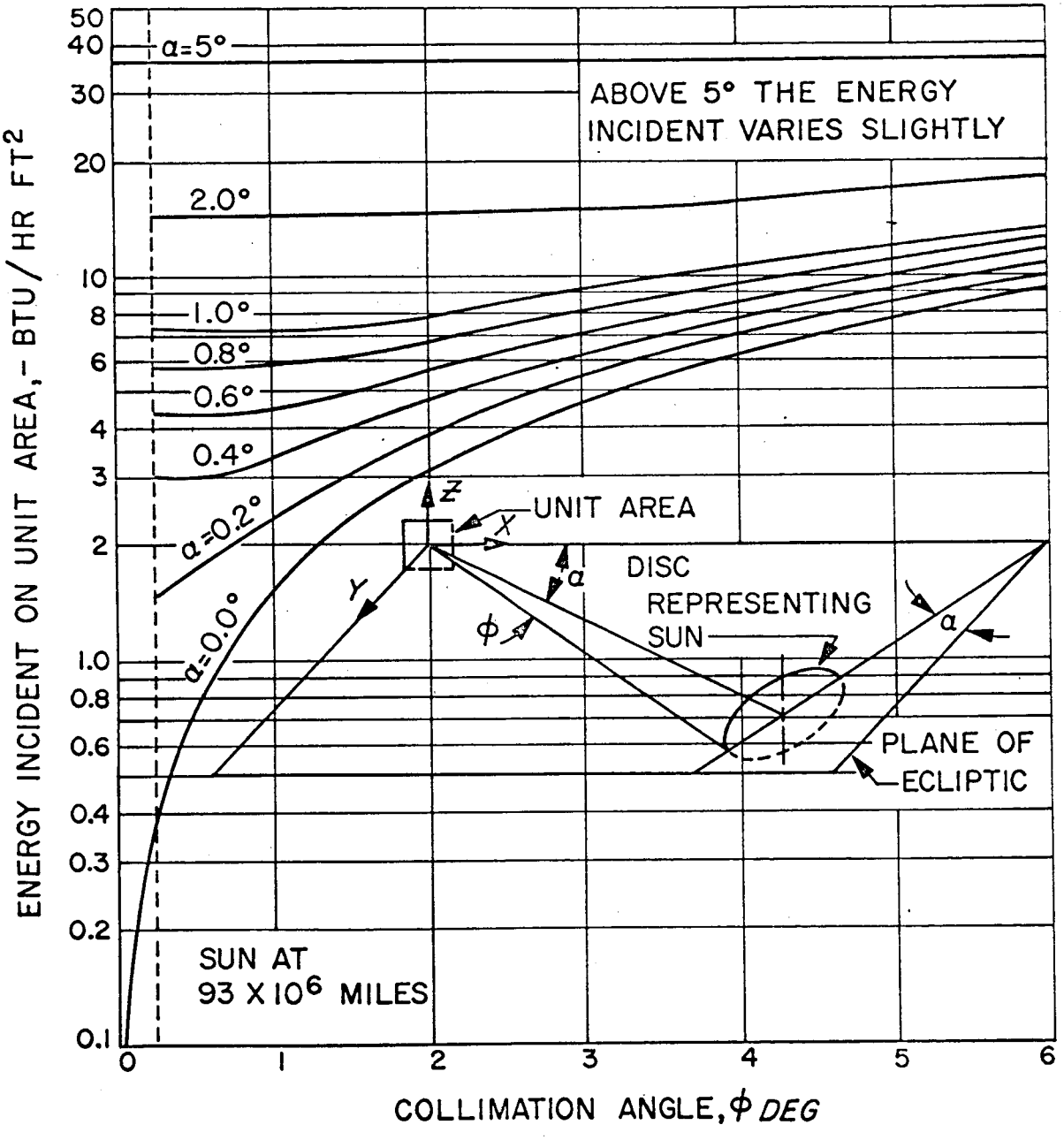

FIGURE 22. Intensity Error Versus Collimation Angle

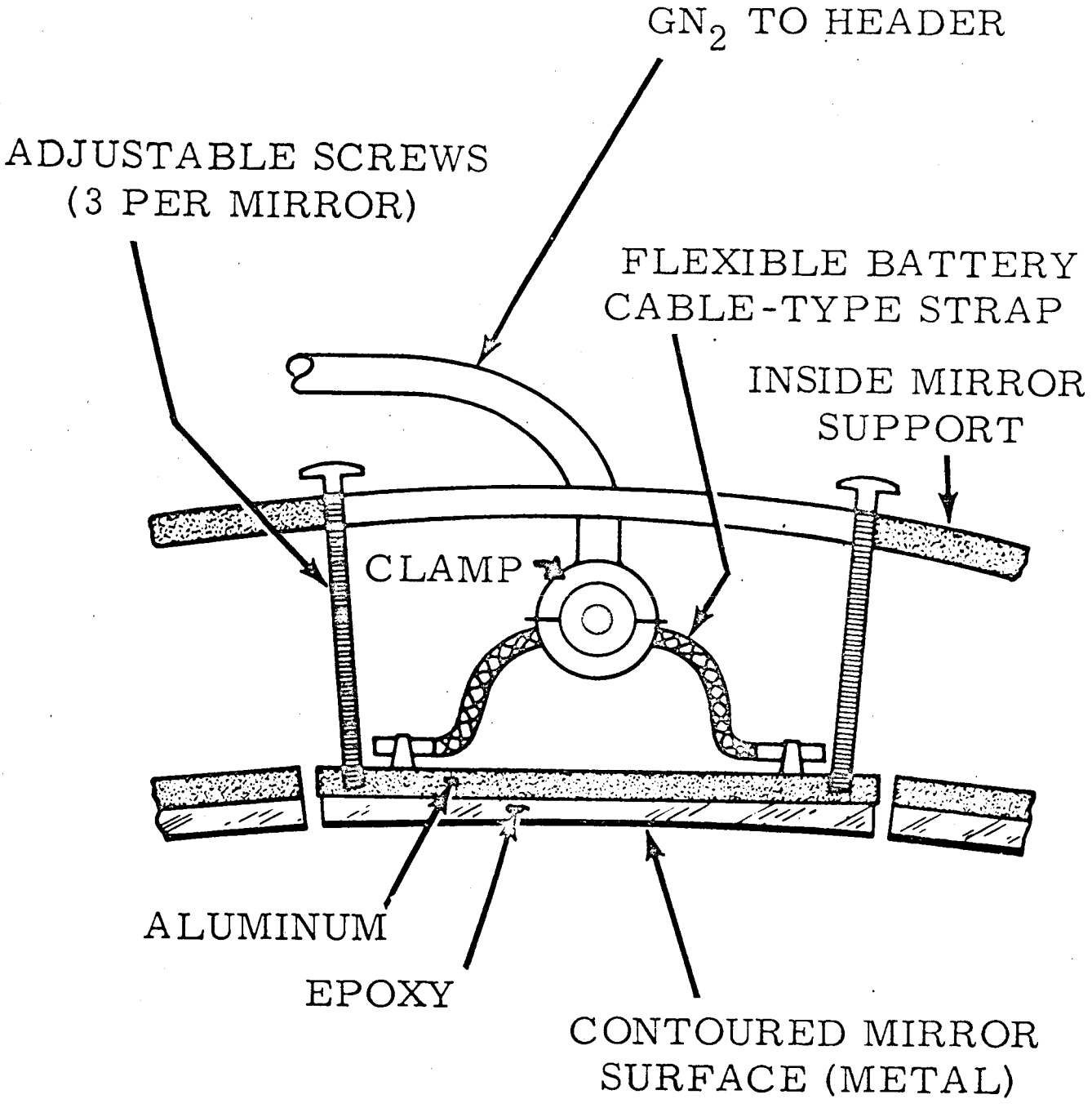

FIGURE 23. JPL 25-Foot Parabolic Mirror Cooling

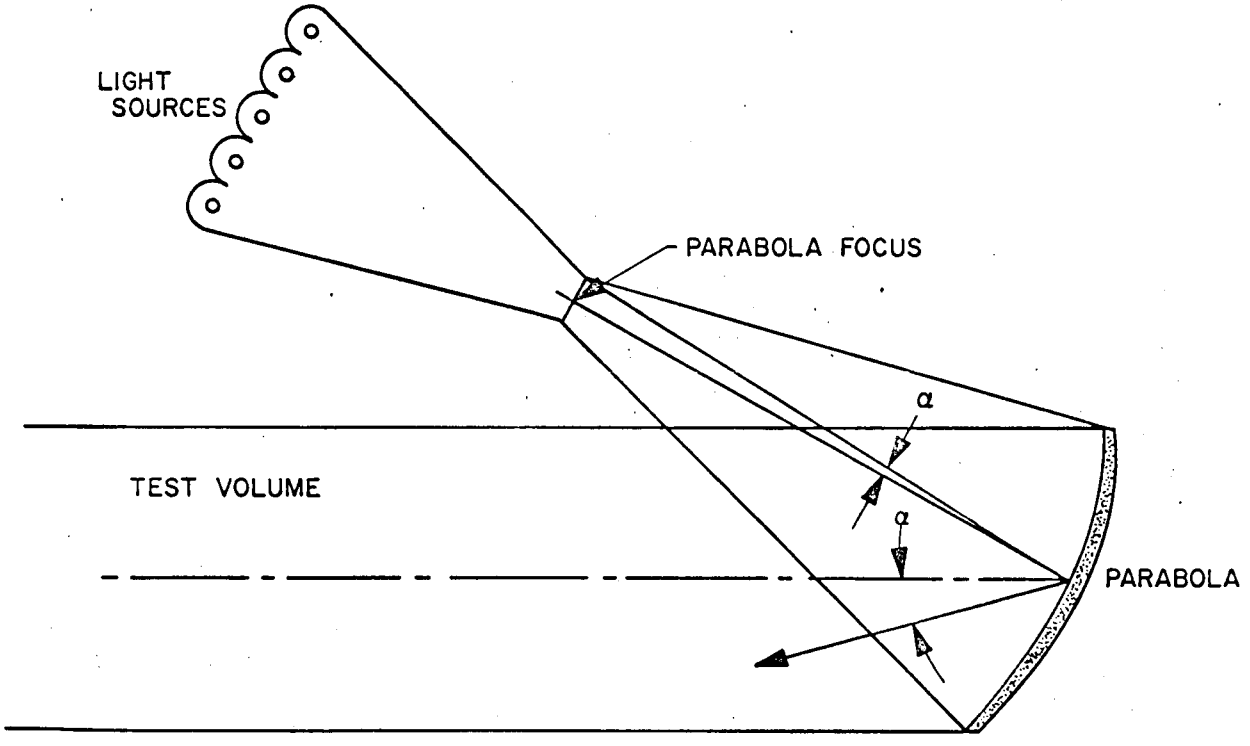

FIGURE 24. Off-Axis Solar Simulation System Schematic

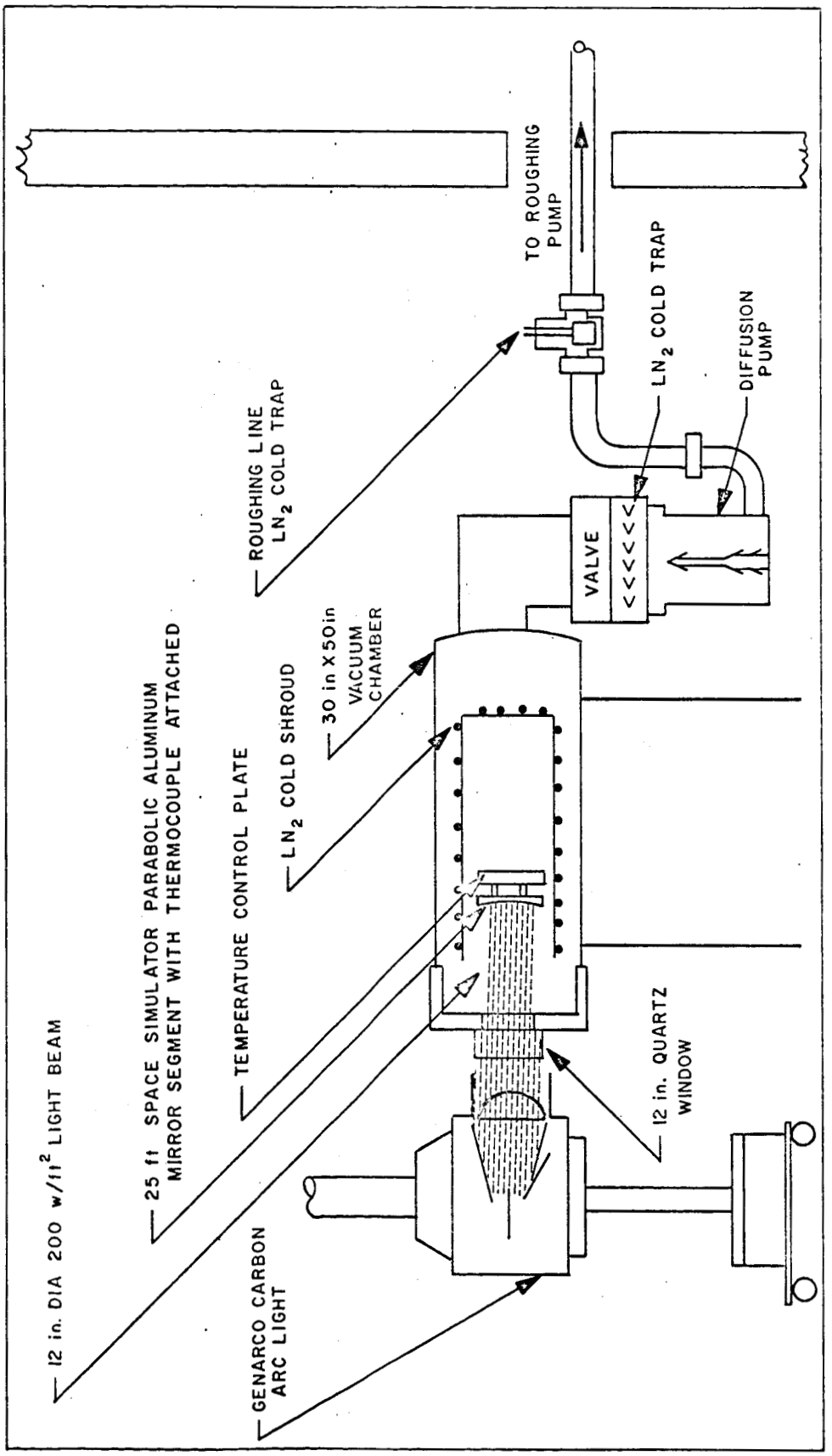

FIGURE 25. Test Setup for Mirror Oil Contamination Experiments

APPENDIX I

INCIDENT ENERGY ON SLOPING SURFACES VS COLLIMATION IN SOLAR SIMULATION

INTRODUCTION

A surface which is parallel to the average flux of a radiating body will receive energy if the radiating body is of finite size. The incident energy on such a surface will increase with the size of the radiating body.

At the present state-of-the-art of solar simulation, it is optimistic to expect resultant energy to be as well collimated as rays from the Sun. It is necessary, therefore, from accurate temperature control considerations, to know the difference in energy flux that a variation in collimation may produce on a given surface. The purpose of this investigation is to furnish such information in an absolute form.

CALCULATION

A scheme to reduce the problem to a simple general analytical case is to consider the Sun as a disc of radius R which furnishes flux density I_N on a unit area normal to the average flux (Fig. 1).

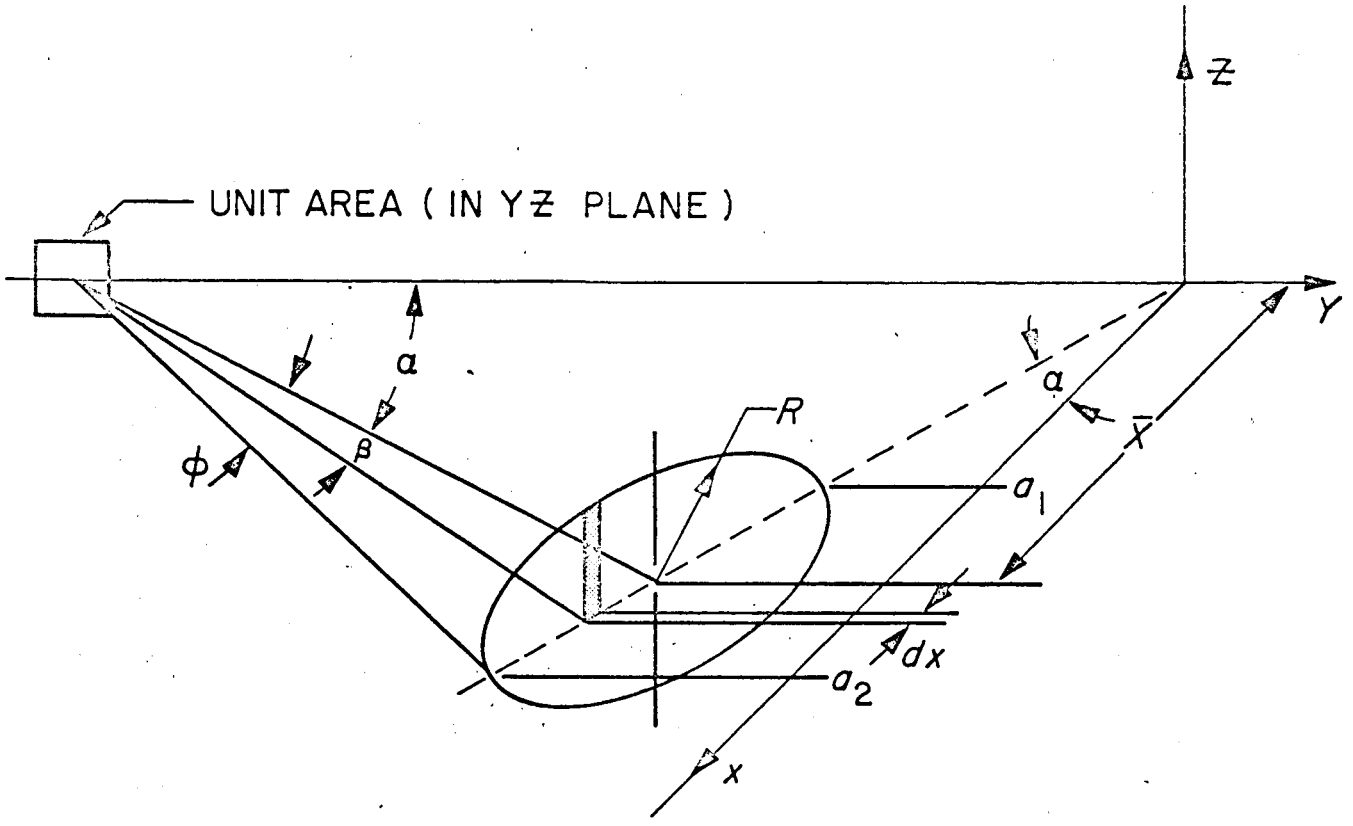

Figure 1

c = distance to disc representing Sun = 93×10^6 mi = 49.104×10^{10} ft

ϕ = collimation angle = $\tan^{-1} \frac{R}{C}$

R = c tan ϕ = radius of Sun disc

A = πR^2 = area of Sun disc--disc is normal to xy plane

α = angle (in xy plane) between unit area and Sun disc centerline

I_N = energy on unit area which is normal to average flux

I = energy on unit area in yz plane

$$z = \sqrt{R^2 - \left(\frac{x - \bar{x}}{\cos \alpha}\right)^2}$$

$\bar{x} = \hat{c} \tan \alpha \cos \alpha$

a_1 = 0, if $\bar{x} \leq R \cos \alpha$ (limit of integration)

$a_1 = \bar{x} - R \cos \alpha$, if $\bar{x} > R \cos \alpha$

$a_2 = \bar{x} + R \cos \alpha$

$$\cos \beta = \frac{c}{\sqrt{c^2 + \left(\frac{x - \bar{x}}{\cos \alpha}\right)^2}} \qquad \sin \beta = \frac{\frac{x - \bar{x}}{\cos \alpha}}{\sqrt{c^2 + \left(\frac{x - \bar{x}}{\cos \alpha}\right)^2}}$$

Energy striking unit area (ΔI) from shaded incremental area $\frac{zdx}{\cos \alpha}$ in Fig. 1:

$$\Delta I = \frac{zdx}{\cos \alpha} \frac{I_N}{A} \sin(\alpha + \beta)$$

$$I = 2 \int_{a_1}^{a_2} \frac{zdx}{\cos \alpha} \frac{I_N}{A} \sin(\alpha + \beta)$$

$$\frac{I}{I_N} = \frac{2}{A \cos \alpha} \int_{a_1}^{a_2} z \sin(\alpha + \beta) dx$$

$$= \frac{2}{A \cos \alpha} \int_{a_1}^{a_2} zdx(\sin \alpha \cos \beta + \sin \beta \cos \alpha)$$

$$= \frac{2 \tan \alpha}{A} \int_{a_1}^{a_2} z \cos \beta dx + \frac{2}{A} \int_{a_1}^{a_2} z \sin \beta dx$$

Use preceding values for $\cos \beta$ and $\sin \beta$. Then

$$\frac{I}{I_N} = \frac{2c \tan \alpha}{A} \int_{a_1}^{a_2} \frac{\sqrt{R^2 - \left(\frac{x - \bar{x}}{\cos \alpha}\right)^2}}{\sqrt{c^2 + \left(\frac{x - \bar{x}}{\cos \alpha}\right)^2}} \, dx$$

$$+ \frac{2}{A \cos \alpha} \int_{a_1}^{a_2} \frac{(x - \bar{x}) \sqrt{R^2 - \left(\frac{x - \bar{x}}{\cos \alpha}\right)^2}}{\sqrt{c^2 + \left(\frac{x - \bar{x}}{\cos \alpha}\right)^2}} \, dx$$

This curve, multiplied by the Earth solar constant, is plotted in Fig. 2 for collimation angles up to 7 deg.

NOTE:
1. Plane of unit area is perpendicular to plane of ecliptic
2. α is measured in plane of ecliptic
3. α is angle measured between the following:
   a. Line of intersection between unit area and ecliptic plane
   b. Line joining center of unit area to center of disc representing Sun

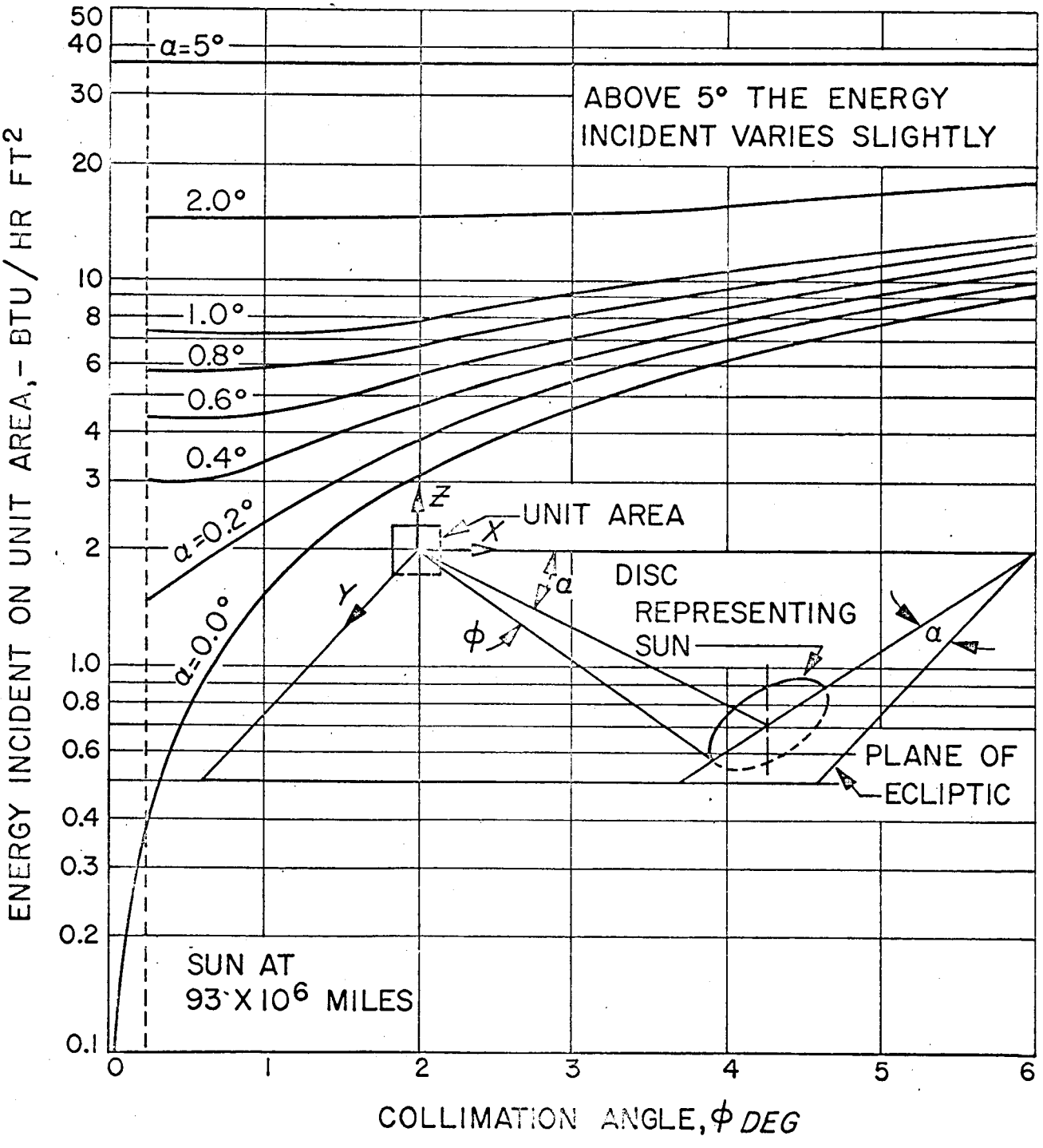

SOLAR SIMULATION
INCIDENT ENERGY VS COLLIMATION
FOR EARTH SOLAR CONSTANT = 420 BTU / HR FT^2